Utrecht University
Faculty of Beta-science

Institute for Marine and Atmospheric research Utrecht

Master thesis

Trends and variability in Temperature profiles taken from Lauder, New Zealand

by
Coen Berntsen
(6038778)

Submission Date: August 14, 2019
Supervisor: Prof. Dr. Guus Velders

Contents

Abstract

Satellite and radiosonde measurements have shown that in the last few decades, globally, mean stratospheric temperatures have decreased. Cooling of the stratosphere is predominantly driven by anthropogenic CO_2 emissions and by decreasing stratospheric ozone concentrations from the 1980's. In the last decade, the stratospheric temperature appears to flatten of. This is suspected to be due to regulations under the Montreal protocol, restricting the emissions of ozone depleting substances and thereby limiting the ozone component in stratospheric cooling. However, research regarding the quantification of the separate contributions of ozone and CO_2 to the cooling is limited. This report describes and analyses temperature profile time series taken by a Lidar instrument, situated in Lauder, New Zealand. It is shown that the Lauder observations contain temperature trends in the upper stratosphere, where increased CO_2 abundance contributes to -0.4 to -1.5 K/dec cooling. In the lower stratosphere, CO_2 component varies from -0.3 to + 0.4 K/dec. Changes in ozone column above Lauder are small, causing ozone to contribute to a trend of approximately +0.1 K/dec. Additionally, the observations were compared with other lidar and sonde measurements. Observations at higher latitudes predominantly show stronger temperature trends than the Lauder observations, varying from a 0.5 to almost 2 K/dec of CO_2 induced cooling. Ozone columns, which are shown to recover at rates of 2% per decade induce a positive temperature trend of up to 0.2 to 0.6 K/dec. Finally, it is shown that models used in the Coupled Model Intercomparison Project 5 (CMIP5) give adequate simulations of temperature trends in the Stratosphere with respect to the observations.

1 Introduction

The earliest studies discussing temperature changes throughout the stratosphere date from the 1960's. In 1967, Manabe and Wetherald used a radiative convective model to describe atmospheric temperature changes under increasing abundance of greenhouse gasses [Manabe and Wetherald, 196
In their article it is mentioned that the warming in the troposphere due to greenhouse gasses will go along with a simultaneous cooling effect in the stratosphere. Manabe and Wetherald, 1967, were the first to describe these cooling effects in the upper atmosphere. Furthermore, they showed the sensitivity of the stratospheric temperature to the ozone profile, claryfing that ozone plays a crucial role in determining the stratospheric temperature.

During the 1970's, several modelling studies with various results were done. A US Government review [Vanderwyk, 1975] indicated Stratospheric cooling of ∼10 K with a 50% ozone column decrease. A few years later, a general circulation model was used for the first time to study stratospheric temperature changes [Fels et al., 1980]. The authors found global stratospheric cooling, with a maximum of ∼ 11 K at the stratopause under doubling CO_2 levels. The amplitude of the global temperature change at the stratopause was is 3-6 times larger than the global mean surface temperature changes in the same simulation, indicating that the upper stratosphere responds stronger to greenhouse gas perturbations than the troposphere.

Since immediate social-humanitarian impact of sea surface temperature change stratospheric chemistry and temperature change received relatively little attention. This changed with the discovery of large scale ozone depletion above Antarctica in 1985 [Farman et al., 1985]. Discovered was that ozone abundance in the stratosphere was steadily decreasing and that during the Antarctic spring, vertical ozone columns thinned from an average of 300 Dobson Units, to 100 DU. The acute threats of the ozone depletion led to new research regarding stratospheric ozone and a rapid increase of knowledge. It was recognized that stratospheric temperature change is a complex interplay between greenhouse gasses and ozone, with influences of external forcings like solar variability, aerosol abundance and oscillations in stratospheric dynamics. Since the stratosphere owns its positive vertical temperature to absorption of solar radiance by ozone, ozone depletion and greenhouse gas emission leads to an cumulative cooling effect. The depletion of ozone, along with the ongoing emissions of GHG's was estimated to have a cooling effect of -1.2 to -1.7 K/dec at the Stratopause, and about -0.34 K/dec in the lower stratosphere [WMO, 1988].

Since the Montreal Protocol became effective, the emission of ozone depleting substances (ODS) decreased. Thereby the destruction of ozone appears to have halted since the 00's [Ajavon et al., 2018]. Signs of recovery of the ozone layer are reported [Maycock, 2016a][Steinbrecht et al., 2
but the ozone increases are not statistically significant owning to large uncertainty. To gain understanding into future temperature changes in the stratosphere under a recovering ozone layer, it is necessary to differentiate the ozone and greenhouse gas signals. [Maycock, 2016b] claim to have isolated the effects of ozone and greenhouse gasses. In their paper, the stratospheric temperature trend is estimated at -1.3 for the upper stratosphere (40-50 kilometres)

to -0.3 K/dec for the lower stratosphere (10-25 kilometres) during the 1979-1997 time period. After 1997, their estimated trends drop to -0.6K/dec in the upper stratosphere and are negligible in the lower stratosphere. According to Aquila et al., 2016, the greenhouse gas signal dominates the trends in the middle and upper stratosphere and is estimated to contribute -0.6K/dec continuously. Ozone is the largest driver up to about 25 kilometres. The contribution of ozone varies from -0.3 to -0.5 K/dec until 1997, and has a small cooling to warming effect from 1997. In the same year, a comparable study by [Mitchell, 2016] found similar trend values in the upper stratosphere as [Maycock, 2016b]. On the contrary, [Mitchell, 2016] were not able to disentangle the O_3 and greenhouse gas effects in the lower and middle stratosphere (<35 kilometres).

Research question

This Master Project will focus on temperature trends in the stratosphere, mainly occurring from 1990s until 2017. To determine these trends, a dataset derived from a Lidar instrument installed by the RIVM, situated in Lauder, New Zealand, is used. This Lidar was initially constructed to measure ozone levels and has been working continuously since 1994. The Lidar is currently being operated by the National Institue of Water and Atmospheric research (NIWA). The data have recently been reassessed by Anne van Gijsel to derive temperature profiles. The profiles extend from the troposphere up to the middle mesosphere (8-70 kilometres). The research questions raised for the research are the following:

1. Do temperature trends exist in the Lauder profiles? If so, what is their magnitude and how do they compare to previous research. Analysis of the timeseries is done using a trend model.
2. Is it possible to distinguish the different contributions of ozone and greenhouse gasses? Since the restrictions of ODS emissions became effective, this must have had implications on the temperature in the stratosphere. To understand future temperature changes it is important to be able to distinguish ODS effects on one hand and CO_2 signals on the other.
3. How does the Lauder timeseries compare to CMIP5 models? Comparison of the Lauder timeseries to the CMIP5 models shows how the model performs against scenario runs and gives insight in the validity of the CMIP5 predictions.

The reason for commencing this research is threefold. Firstly, as mentioned before, Fels et al., (1980) found that the stratospheric response to greenhouse gas perturbations are several times larger than in the troposphere. Additionally, lack in turbulence, low moisture content and relatively easy dynamics in the stratosphere compared to the troposphere, might make it easier to distinguish a trend from background noise and internal variability. In other words, the signal to noise ratio in the stratosphere is assumed to be lower and therefore the detectability of a trend, or emergence is expected to be higher. Therefore, detection of temperature trends could help understand the magnitude of greenhouse gas emissions on tropospheric temperatures.

Secondly, previous research on temperature changes in the stratosphere led to the conclusion that the stratosphere is cooling. However, the magnitude of cooling and the separate contributions of the ozone signal compared to the greenhouse gas signal differs considerably from study to study. By using a robust dataset, this research tries to contribute to establishing knowledge in the relative contribution of different drivers.

Thirdly, although the stratospheric air mass consists of only 15% of the total air mass, changes in stratospheric temperature does have implications for tropospheric weather. Stratospheric zonal jets and tropopause jetstreams are both driven by meridional temperature gradients in the atmosphere. The effect of stratospheric temperatures on the midlatitude jetstream is not clearly known although it is expected that stratospheric temperatures influence the strength of the jetstreams. The zonal stratospheric jet do directly influence the strength and location of the jetstreams and thereby influence surface weather. Latitudinal shifts of the jetstreams occurs in response to increase or decrease in zonal flow of the stratospheric jet [Kidston et al., 2015]. A latitudinal shift of the jetstream has implications for the weather patterns present at the midlatitudes.

This report will first describe the theoretical background in chapter 2. This chapter elaborates on the factors influencing stratospheric temperatures and introduces the principles of the trend model that is used for the analysis. Chapter 3 gives a brief summary on the history of evolution on stratospheric research, describes the methods used to derive the temperature profile from the Lidar system and describes the CMIP5 models used for analysis. Chapter 4 will present the results, followed by a discussion in Chapter 5.

2 Theoretical framework

2.1 Stratospheric Temperature

The temperature distribution in the atmosphere is the result of an interplay between radiative heating and cooling and dynamical redistribution of heat. In the troposphere, where most of the radiation is absorbed by the surface, water vapor plays an important role in distributing heat. Latent and sensible heat fluxes transport heat from the surface in the vertical direction. Additionally, surplus in heating is transported in the meridional direction via synoptic-scale eddies. These heat-fluxes seek to decrease temperature gradients in the troposphere. Temperature gradients in the troposphere are generally negative in the vertical and meridional direction. In contrast to the troposphere, latent heat does not play a large role in determining the stratospheric temperature. The thermal structure in the stratosphere is in a large part determined by radiative balance, induced by the important chemical constituents in the stratosphere. The thermal structure of the stratosphere is in a large part determined by a balance between longwave radiative cooling and absorption of shortwave solar radiation, a radiatively determined state. Absorption of solar radiation occurs in principle by ozone and oxygen. The absorption of solar radiation results in a positive mean temperature gradient with height in the stratosphere. Also, the meridional temperature structure in the stratosphere is rather different than that in the troposphere. The lower stratosphere (until $\tilde{3}0$ hPa or 27 km) is influenced by the troposphere and shows a temperature maximum around the poles of the summer and midlatitudes of the winter hemisphere. Temperature minima are found at the equator. Above 30 hPa, the temperature decreases uniformly from the summer pole to the winter pole, following the gradient of influx of solar radiation. Although radiative processes are dominant in the stratosphere, dynamical effects are still important in distributing heat. Additionally, temperature deviations on short timescales are also impacted by dynamical processes. We will first describe the radiative processes, including the important stratospheric gasses when it comes to absorption and emission of energy. After that, dynamical processes occuring in the stratosphere will be discussed.

2.1.1 Radiative transfer

Quantification of the energy balance in the stratosphere is done using radiative laws. The cross section σ as specified in figure 2.2 is the effective area for molecules to remove energy from a incident light beam. The cross section is dependent on wavelength λ. To find the strength of a spectral band, a simple integral over wavelength is sufficient $S = \int \sigma d\lambda$. The cross section is related to the absorption coefficient k according to $k = N_a\sigma$. In which N_a is the number density of the absorbing molecule. The absorption coefficient describes the fraction of radiation which is attenuated at a specific length unit. When a light beam is incident on a certain layer with thickness $\Delta z = z_0 - z_1$, the radiance (in energy per unit time per unit area) thus changes as $\Delta F = F_{z0} - F_{z1}$:

$$F_{z_1} = -F_{z_0}(1 - k\Delta z)$$

Finding the limit for dividing the medium into infinite layers (see figure 2.1), the radiation after passage trough the medium is described as:

$$F_{z_1} = F_{z_0} e^{-kz}$$

Here, kz is referred to as the optical path: τ. An medium with length $z = 1/k$ has an optical path of 1 and will attenuate the radiation by a factor of $1 - 1/e = 0.68$. Using formula 2.1.1, the attenuation of radiation within the atmosphere can be obtained, thereby deriving the incident radiation for every altitude in the stratosphere.
Now that we know how to describe the capability of a gas to absorb energy we can apply this to incoming solar radiation to determine the amount of heating generated. To do this, we need to find the incident solar radiation in every layer and calculate the heat generated by absorption for every wave frequency. This is a tedious integration process which was firstly done by [Manabe and Wetherald, 1967]. To calculate a monochromatic solar flux, within every atmospheric layer, the attenuation is calculated via:

$$S(z) = \mu_0 S_0 e^{-\tau(z)/\mu_0}$$

Here, μ_0 is the cosine of the incident angle for a beam of solar radiation $\cos\theta$, S_0 is the incident solar irradiance. This equation can be used to calculate energy absorption by integrating over wavelength for every layer. The rate of energy absorption is then expressed as:

$$\rho h_r(z) = \mu_0 \int S_{0v} \frac{d}{dz} e^{-\tau_v(z)/\mu_0} dv$$

Via this equation, heating associated with absorption of solar radiation can be calculated for every molecule, provided one knows the absorption bands. Solar radiation reaching an atmospheric layer not only comes directly from the sun but is also via surface reflection and Rayleigh or aerosol scattering. Especially aerosol scattering processes are sources for large variability and sudden changes. Examples of these are volcanic eruptions which lead to abrupt increases of Stratospheric temperatures with several degrees.

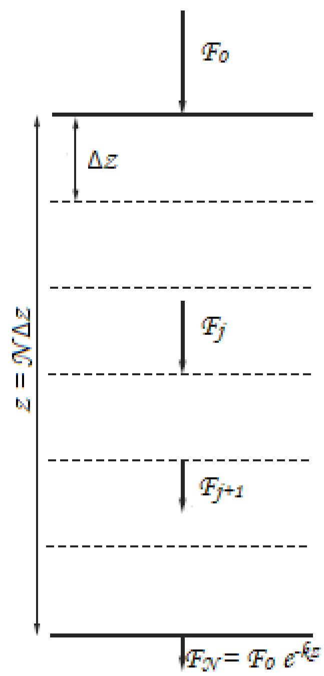

Figure 2.1: *Radiation passing through medium. Adapted from Bohren et al., (2016)*

Molecules absorbing shortwave radiation will also emit radiation. The power radiated is given by the Stefan-Boltzman law, which states the energy radiated per surface area of a black body across all wavelengths. The Stefan-Boltzmann law is given by: $J = \epsilon\sigma T^4$. Here σ represents the Stefan-Boltzmann constant ($5.67010^8 Wm^{-2}K^{-4}$) which specifies the radiated energy per surface area. This is multiplied by an emission coefficient ϵ and the fourth power of temperature. The emission coefficient is generally assumed to be equal to the absorption coefficient, according to Kirchoff's law. To find the most dominant wavelengths, emitted at a specific temperature, assuming the emitter is a black body we need Planck's law. Planck's law describes the spectral density for electromagnetic radiation at different wavelengths by a black body at a certain temperature. For typical atmospheric temperatures, the spectral density is highest in the infrared spectrum.

Besides emitting, some molecules also have absorption bands in the longwave spectrum and can thereby also warm the stratosphere via longwave absorption. These greenhouse gasses absorb the upwelling radiation from the warmer, lower troposphere and re-emit this into all directions. The net energy radiated combined with the specific heat leads to a heating rate. The contribution of longwave radiation is cooling, in which the cooling increases with height. When the heating and cooling of the stratosphere is calculated on daily timescales, the net heating of the stratosphere due to radiation is about a few kelvins in the summer hemisphere, and up to -8 K/day in the winter hemisphere [Lacis and Hansen, 1973][Andrews et al., 1987]. Around the (sub-)tropical latitudes, net warming is about zero degrees.

Chemical constituents

Stratospheric chemistry is dominated by ozone, carbon dioxide, water vapor, oxygen, aerosols and ozone depleting substances, being mainly of the form $HCL+$. The stratosphere has a comparable chemical composition as the troposphere for O_2, and CO_2, O_3, H_2O and ODS's have different abundances in the stratosphere as compared to the troposphere. Additionally, the presence larger presence of O_3 in the Stratosphere and its absorption of shortwave radiation leads to a different role of CO_2 under an increasing anthropogenic emissions than in the troposphere.

Ozone is fundamental in determining the stratospheric temperature distribution [Seinfeld and Pandis, 2016] Ozone is formed by photodissociation of oxygen by electromagnetic waves of low wavelength ($\lambda < 242nm$). Destruction of ozone also occurs via photodissociation. The reactions showing the creation and destruction of ozone in the stratosphere are by the reaction scheme of equation 2.1.1. This reaction scheme is called the Chapman cycle [Seinfeld and Pandis, 2016]. In this cycle, there is no net creation and destruction of ozone. Within the Chapman cycle, reactions (2) and (3) occur at much faster rates than reactions (1) and (4). This leads to a quasi steady state of ozone in the stratosphere in which ozone is being recycled as short wave radiation is being absorbed.

$$(1)\ \mathrm{O_2} \xrightarrow{hv} \mathrm{O(^3P)} + \mathrm{O(^3P)}$$

$$(2)\ \mathrm{O(^3P)} + \mathrm{O_2} \longrightarrow \mathrm{O_3}$$
$$(3)\ \mathrm{O_3} \xrightarrow{hv} \mathrm{O} + \mathrm{O_2}$$
$$(4)\ \mathrm{O(^3P)} + \mathrm{O_3} \longrightarrow 2\,\mathrm{O_2}$$

The concentration of ozone is highest at approximately 27 kilometres altitude, with concentrations of about $9 * 10^{12}$ molecules cm^{-3}. By absorption of solar radiation, ozone warms the stratosphere. However, emission of longwave radiating also contributes to cooling (see figure 2.3). The absorption spectrum of ozone is shown in figure 2.2, left panel. Absorption by ozone takes place in three 'bands'. Within the wavelength of these bands, dissociation of ozone is close to unity. The Hartley band extends from 200 to 310 nm and blends smoothly into the Huggins band at 310 to 350 nm. The Chappius absorption band extends within the visible spectrum from 440 to 800 nm. The Chappius absorption band has only a minor contribution to energy absorption in the stratosphere. The first two absorption bands of ozone are responsible for the major part of energy absorption and heating the stratosphere.

Carbon dioxide is a greenhouse gas with a strong absorption band, peaking at 15 μm. However, at the same time, carbon dioxide has the strongest component of radiative cooling in the stratosphere, of about -8 K/day at the stratopause [Andrews et al., 1987], see figure 2.3. To understand the cooling effect of increasing CO_2 two effects have to be taken into account: The 'blocking effect' and the 'indirect solar effect' [Goessling and Bathiany, 2016]. The 'indirect solar effect' refers to the fact that when an solar heating term is present in the radiative balance, as is the case in the stratosphere due to ozone absorption. Increase in the concentrations of long wave emitters, like CO_2, result in a stronger contribution of longwave emission, thereby cooling the stratosphere. The blocking effect is due to the reduced upwelling in an atmosphere that becomes optically thicker when less longwave radiation is upwelling and reaches high altitudes. Looking at figure 2.1, this can be seen as the optical path of the atmosphere increasing, thereby attenuating the radiation stronger. At the same time, CO_2 increase leads to higher emission of radiation, which can easily escape to space from the stratosphere but not from the troposphere. Although Goessling et al., (2016) estimate that the indirect solar effect is dominant in the higher stratosphere whereas the blocking effect is more important in the lower stratosphere. Only the indirect solar effect seems to have a significant influence on the temperature since the difference in upwelling due to increase in CO_2 concentrations is low [Andrews et al., 1987].

O_2 is important not only for the creation of ozone in the Chapman cycle, but also by absorption of solar radiation. O_2 has a constant abundance throughout the stratosphere of about 21%. The absorption band of oxyen lies at higher wave frequencies than that of ozone (see figure 2.2, right panel). This means oxygen will mainly absorb and dissociate in the upper stratosphere up to the mesosphere. The contribution of absorption by oxygen molecules on the stratospheric temperature therefore only plays a role in the upper parts of the stratosphere but is more important in the mesosphere.

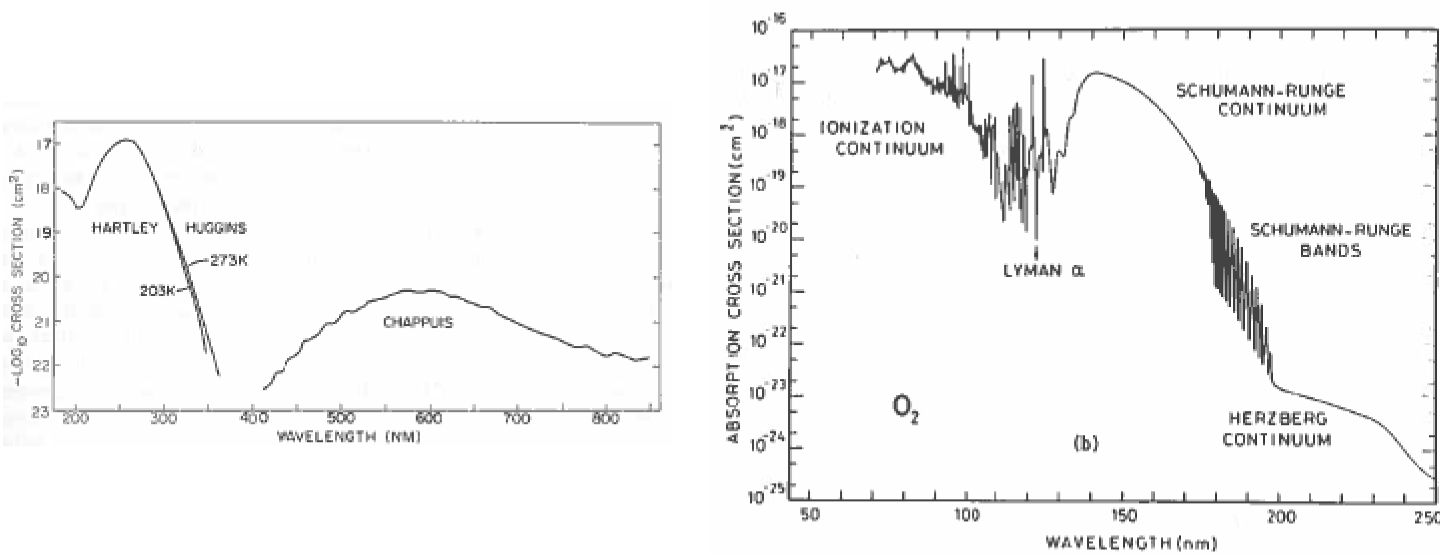

Figure 2.2: *Absorption spectra for ozone (left panel) and the dominant, UV absorption spectrum of oxygen (right panel). Logarithmic cross section as a function of wavelength. From Bohren et al., (2006)*

Water vapor is a greenhouse gas with a higher warming potential per molecule than CO_2. However, the stratospheric abundance of H_2O is much lower than that of CO_2 (3-5 vs 410 ppm) and thus, water vapor has a much smaller influence on the temperature distribution in the stratosphere. Changes in water vapor levels might have significant impact on the stratospheric temperatures [Maycock et al., 2014], [Maycock et al., 2011]. Due to the low background level of H_2O in the stratosphere, the distribution of heating that results from an increase in water vapor will be different from that of CO_2. This also makes the stratosphere relatively transparent to the water vapor absorption band compared to CO_2 absorption band. This means radiation can more easily escape to space and the difference in heating due to H_2O between the lower and upper stratosphere will not be as strong as due to CO_2. For CO_2, the optical path of the stratosphere, although already low, will still thin considerably upward.

Aerosols also play a role in the stratosphere. aerosols can either work as absorber or reflector. Their properties mainly depend on the shape, color, composition and size of the aerosols. Causes of aerosols in the stratosphere are diffusion from the troposphere, direct anthropogenic emissions into the stratosphere via aircraft and volcanic emissions. Volcanic eruptions eject enormous amounts of sulfuric acid aerosols into the stratosphere. These aerosols have a cooling effect on the troposphere but a warming effect on the stratosphere. Episodes of volcanic eruptions have been studied in the past with eruptions of El Chichon and Pinatubo [Angell, 1993], [Angell, 1997]. These eruptions led to sudden stratospheric temperature increases up to 2 Kelvin. However, the warming is only temporarily as the aerosols will deposit relatively fast. Additionally, aerosols are necessary in the formation of polar stratospheric clouds, surfaces on which chlorine molecules can deposit. Chlorine molecules are crucial in the catalytic ozone destruction mechanism.

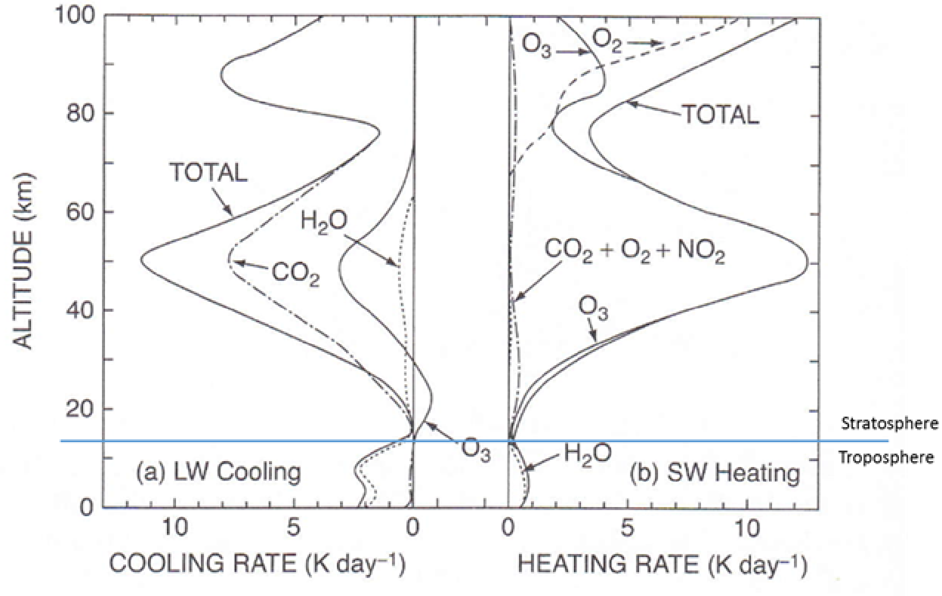

Figure 2.3: *Contribution of different stratospheric consituents to cooling and heating in the stratosphere. Taken from Salby et al., (2012)*

.

2.1.2 Dynamical structure of the stratosphere

To understand stratospheric temperature distribution and perturbations, understanding in stratospheric dynamics is crucial [Holton, 2004]. An overview of stratospheric dynamics is ideally divided into a primary zonally symmetric circulation and a secondary eddy driven circulation. This secondary circulation has both meridional and vertical components. In the absence of eddy motions, the stratosphere would relax to a radiatively determined state. In this case the temperature of the stratosphere would almost purely be determined by the chemical elements present in the stratosphere. The observed stratospheric temperatures closely resembles the radiative determined state around the tropics and subtropical latitudes. This is not the case for the mid-latitudes and polar regions [Holton, 2004]. The summer pole temperatures are below wheras the winter pole temperatures are above those that the radiative determined state implies. Observed d eviations from the radiatively determined state can be explained by dynamical components in the stratosphere.

Polar Jets

In a stratosphere under radiative equilibrium, the circulation in the stratosphere would only have zonally mean zonal components in thermal wind balance [Andrews et al., 1987]. The zonal winds are a dominant feature in the stratosphere and part of the 'primary circulation'. The stratosphere exhibits two bands of strong zonal winds, or jets, in each hemisphere. A subtropical jet is located just around the tropopause at 200 hPa and 30^o latitude. This jet has a continuous eastward component which weakens and moves poleward during the summer. A polar night jet is located at approximately 60^o North and South. The polar night jet is strongest in the polar winter, when the flow is directed eastward. However, during spring, this jet fall apart and reverses its flow. The jets are associated with a geopotential minimum at the 30 hPa level for the cyclonic jet and a geopotential maximum for the anticyclonic jet. The jet vortices are persistent, especially during the winter. The strength of the cyclonic polar night jet prevents mixing of polar air with equatorial air. This plays an important role in the process of ozone destruction during spring (Solomon Matard, 1990). It isolates the polar air mass in the winter and early spring, preventing ozone to mix in from lower latitudes. In combination with very low temperatures and the formation of polar stratospheric clouds (PSC), ozone depletion takes place via catalytic reactions with chlorine, which is accumelating due to deposition on the PSC surfaces. In some years, the polar jets are being disrupted. This causes the stratosphere to warm up by tens of degrees. These events are referred to as Sudden Stratospheric Warmings (SSW's). Disruption of the jets are caused by upward propagation of planetary Rossby waves. Tropospheric Rossby waves are forced by meridional temperature gradients in the troposphere, ocean-land contrasts and forced upward motion of air over mountain ranges. Since the latter two forcings are much more prominent in the Northern-Hemisphere, Rossby waves are better able to penetrate to the arctic jet than the antarctic jet. This explains the difference in frequency of occurence of Sudden Stratospheric Warmings in the Northern and Southern Hemispheres. SSW's occur on average once every ten years in the Northern Hemisphere, but only one Sudden Stratospheric Warming has been observed above the South Pole, this was in 2002 [Varotsos, 2004].

Brewer Dobson circulation and the Quasi Biennial Oscillation

The stratosphere exhibits a meridional circulation, known as the Brewer Dobson circulation [Seinfeld and Pandis, 2016]. The upper branch of the Brewer Dobson circulation is a net pole-

ward flux and a response to a negative flux of angular momentum, transported by planetary waves. Via wave drag, the midlatitude planetary waves lower the angular momentum which has to be conserved via polar flow which brings air with higher angular momentum from lower latitudes to higher latitudes. Positive meridional flow in the upper stratosphere results in air upwelling from the troposphere at the tropics and downwelling in the polar latitudes. Since planetary waves are stronger during winter, the Brewer Dobson Circulation is strongest in the winter hemisphere. The Brewer Dobson circulation explains why ozone concentrations are higher at high latitudes, although ozone production is higher at low latitudes. Additionally, it explains the low partial pressure of water vapour in the mid to polar latitudes for the air has travelled through the tropical tropopause, which is the coldest area in the stratosphere-troposphere and thus depleted the air of water vapor.
the Quasi Biennial Oscillation (QBO) is an alternation of westerly and easterly wind regimes with a period of about 24 to 30 months. These regimes are zonally symmetric about the equator and have a maximum amplitude of 20 ms^{-1}. The transition from wind regimes appear first at altitudes of about 30 kilometres height and then propagate downward until about 20 kilometres height [Holton, 2004]. From there, the amplitude of the oscillation quickly decreases. The Quasi Biennial Oscillation influences the secondary (Brewer Dobson) circulation and thereby alters poleward transport of ozone. Also it is debated that different regimes correspond with increased chances on specific tropospheric weather patterns [Matthes et al., 2010].

3 Methodology

3.1 Network for Detection of Atmospheric Composition Change

Measurements of the stratosphere started in the 1950s using rockets and mainly radiosondes [Seidel et al., 2011]. Radiosondes were useful for creating continous profile from the surface upwards, however, they were restricted to heights of approximately 35hPa (which corresponds to $\tilde{3}0$ kilometres). The stratopause is situated at about 1 hPa, roughly 50 kilometres. Radiosondes were thus only able to collect data from the lower to middle stratosphere. Additionally, radiosondes were launched at specific locations, sparsely and not evenly distributed across the Earth, meaning poor spatial resolution of the measurements. The confined applications of Radiosonde measurements caused observations gathered on the stratosphere to be limited until the late 1970's.

Introduction of satellites greatly improved spatial distribution and resulted in near-global coverage. From 1979, the meteorological satellite TIROS-N started to take measurements as a part of the Televison Infrared Observational Satellite program, operated by NASA and NOAA. TIROS-N was mounted with a Stratospheric Sounding Unit (SSU). The SSU uses carbon dioxide absorption and emission of infrared radiation to measure temperature profiles of the stratosphere [Seidel et al., 2011]. These measurements occur in three different altitude ranges, each spanning a different part of the stratosphere. The temperature profiles are derived from a weighting function, which spreads around the peak sensitivity for every channel. The peak sensitivities of the SSU are $\tilde{3}0$, $\tilde{4}0$ and $\tilde{4}5$ kilometres altitude. The TIROS-N was also equiped with a Microwave Sounding Unit (MSU) which are based on oxygen absorption of microwave radiation [Seidel et al., 2011]. Temperature profiles from the Microwave Sounding Units span from the surface to the lower stratosphere at about 25 kilometres. SSU's and MSU's were updated with newer versions of TIROS satellites but they were at first place designed for weather forecasting purposes rather than trend detection or temperature analysis. Timeseries derived from the SSU and MSU (which was later superseded by the Advanced MSU) are a collection from different satellites. The different instruments have different corrections and require separate calibration. Several papers have tried to give an accurate temperature timeseries of the SSU and MSU datasets [Maycock et al., 2018],[**?**], [Mitchell, 2016]. Stratospheric temperature trends detected are largely based on these derived timeseries.

As mentioned earlier, Stratospheric temperature and chemistry received relatively little attention until the discovery of the impact and depletion of ozone. The influence of anthropogenic activities on the stratosphere and implication of these changes became more clear. This led to a increased need for monitoring changes of the stratosphere and understanding of the processes which drive changes. To meet the increased research needs, the Network for the Detection of

Detection of Atmospheric Change (NDACC) was established[1]. The NDACC formally began operating in 1991, combining ground based stations across the world to work together intensively. The NDACC persues to gain global increase in knowledge for stratospheric changes by connecting different working groups and instruments. The main goals of the NDACC can be summarized as follows:

1. Study temporal and spatial variability in the atmosphere to detect changes and trends in composition and physical entities.
2. Investigate the links between these changes in composition on climate in stratosphere and troposphere
3. Validate and calibrate satellite measurements with ground based instruments and provide additional data.
4. Support reasearch focused on processes occuring on specific latitudes.
5. Produce data sets for testing and improving chemistry and transport models of troposphere and stratosphere.

The observations used in this thesis originate from Lauder, New Zealand. Lauder is located at 45^oS and 169.7^oW and is one of the primary stations of the NDACC. The New Zealand Institute for Water and Atmosphere (NIWA) hosts the site in Lauder. Ozone profile measurements started by the NIWA and NOAA by 1987. Cooperation with the Dutch Insititue for Public Health and Environment (RIVM) began in 1994. The NDACC approached the RIVM to develop a Lidar, to be used at Lauder, since expertise was lacking to develop and maintain a Lidar instrument in New Zealand. The instrument was installed in 1994, with the purpose to measure ozone. Lauder is known for its clear sky conditions and therefore particularly useful for Lidar measurements, which are disturbed by high water vapour content in the air.

3.2 Lidar Temperature derivation

Light Detection and Ranging (Lidar) instruments are globally used for measuring vertical profiles of atmospheric constituents and quantities. A basic Lidar setup is given in figure 3.1. The transmitter contains a laser which sends light pulses of specific spectral properties into the atmosphere. At the receiver, a telescope lens collects photons backscattered by the atmosphere. An optical analyzer selects specific wavelengths out of the received light.
The Lidar installed in Lauder was originally constructed to measure ozone profiles using a Differential Absorption and Lidar (DIAL) [Swart et al., 2002]. DIAL uses the wavelength dependence of absorption to differentiate the photons received via backscattering of a tracer molecule from other air molecules and aerosols. Two different light pulses are shot into the atmosphere, one with a wavelength within the absorption band of ozone (λ_{on}), one outside this absorption band (λ_{off}). In order to calculate the number densities of ozone at different heights, only elastic scattering is accounted for which does not alter the wavelength of the incident light.

[1]Initially, in 1991, NDACC was formed as Network for Detection of Stratospheric Change (NDSC), this was renamed later

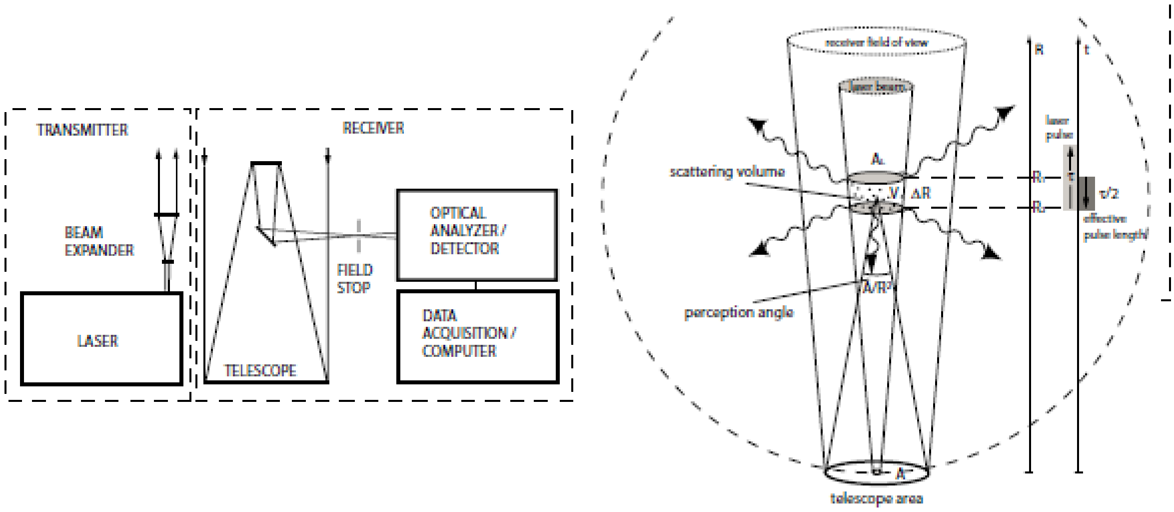

Figure 3.1: *Illustration of an elementary setup of a Lidar system and the geometry of the laser beam. Illustrations taken from [Behrendt, 2005]*

The values used for ozone concentrations can also be used to calculate temperature profiles. To calculate these, the Lidar equation is used, which connects the amount of backscattered photons to number density. The amount of backscattered photons received by the receiver depends on properties of the Lidar instrument itself and properties of the atmosphere. Following [Behrendt, 2005], properties of the Lidar instrument are its efficiency, intensity of the light pulse, area of the receiver, summarized by $L_{z,\lambda_1,\lambda_2}$ in equation 3.2 . Atmospheric properties determining the amount of photons received are the Rayleigh backscatter coefficient and the atmospheric transmission both upward and downward (τ_{up} and τ_{down}). The transmission is determined by the Lambert-Beer law as explained before and states the fraction of signal lost due to extinction along the travel path. Rayleigh backscatter is assumed to be isotropic and equals the backscatter angel of 180^o. These factors can be combined to give the following equation:

$$N_{(z,\lambda_1,\lambda_2)} = N_o * L_{z,\lambda_1,\lambda_2} * \tau_{up} * \beta * \tau_{down}$$

The Lidar equation thus gives the received signal per height range interval. Since the scattering ratio, given by is a function of the number density ($= \sigma_a * N_z$), reversing equation3.2 with respect to gives an description of the number density for a specific height. Following [Hauchecorne and Chanin, 1980] and [Leblanc et al., 2016], to calculate temperature profiles, the atmosphere is assumed to be in hydrostatic equilibrium. A assumed constant mixing ratio of the major atmospheric constituents and a negligible concentration of water vapour at altitudes measured allow a constant value for the air molecular weight. Temperatures can then be calculated via a small adjustment of the hydrostatic equation:

$$T(z_i) = \frac{Mg(z_i)}{R \ln \frac{P(z_i - \Delta z/2)}{P(z_i + \Delta z/2)}} \Delta z$$

The density profile, determined by the Lidar equation can then be used to iteratively solve the pressures at the top and bottom of every layer and consecutively the corresponding temperatures. Pressure at the top of the profile is usually estimated via models [Hauchecorne and Chanin, 1980].

3.3 CMIP 5 models

One of the aims of this thesis is to compare the lidar temperature results with model outcome of different models, part of the Coupled Model Intercomparison Project, phase 5 (CMIP5). This intercomparison project was part of the workgroup I of the IPCC's fifth assessment report (AR5), published in 2013. Since the models used for CMIP5 vary significantly in resolving stratospheric chemistry and dynamics, the choice for a particular model has to be motivated properly. Since ozone plays such a large role in the stratosphere, models interactively solving stratospheric ozone are used for comparison. Interactive means that the ozone concentrations are calculated "online" by the model rather than using a database from observed or separately modelled data as an input. The interactive models also allow for feedback processes to occur which also happen in the stratosphere, changes in chemical reaction speeds due to temperature changes or responses on external forcings like volcanic aerosols. [Eyring et al., 2013] contains a table with an overview of different models and how they treat ozone chemistry. From this table, four models were chosen for comparison with the stratospheric temperature data.

1)**MIROC-ESM-CHEM:**
Developed by the University of Tokyo. Resolves atmospheric chemistry at 32 different levels, up to .03 hPa ($\sim$ 38 kilometres) [Watanabe et al., 2011].
2) **NASA-GISS-E2:**
Developed by the NASA Goddard Institute. Resolves atmospheric chemistry at 17 levels up to 10 hPa (26 kilometres) [Shindell et al., 2013].
3) **NOAA GFDL-CM3:**
Created by the Geophysical Fluid Dynamics Laboratory of the National Ocean Atmosphere Administration. Resolves atmospheric chemistry at 23 levels, up to 1 hPa ($\sim$ 32 kilometres) [Donner et al., 2011].
4) **CESM1:** Community Earth System Model, developed by the NCAR. This model has two different members: FASTCHEM and WACCM. Both explicitely solve ozone chemistry, FASTCHEM up to 10 hPa, WACMM up to 0.4 hPa ($\sim$ 34.5 kilometres) [Gent et al., 2011].

None of the models contain daily vertical profiles for ozone and temperature at different altitudes. Therefore the monthly mean values are chosen to be compared with the Lidar data. Modelling groups, responsible for a model perform their own experiments. However, the CMIP5 obliges modelling groups participating in the project to perform runs in which initial conditions are specified by working group 1 of the IPCC. This allows comparison of outcomes from different models under same initial conditions. For every run, different ensemble members exits, each member consists of particularly specified initial conditions. To compare model runs, the historical experiments are used. Historical runs start in 1850 and run until 2005 and are used to compare model outcome to observed evolution of climate variables. This gives some sort of knowledge on where the models deviate from observations and give clues to limitations of the models. Imposed are observed emissions due to natural and anthropogenic forcings, also solar forcing, emission of short lived species, aerosols and their precursors and land use change are imposed. The models have different resolutions both in the vertical and the horizontal. For this study, stratospheric temperatures will be extrapolated from nearby grid cells and to heights corresponding with the Lidar measurements.

3.4 Trend Analysis

The primary aim of this thesis is to detect whether the Lauder stratospheric temperature profiles inhibit any trends. To discover a trend, a simple trend model is used. A trend model for stratospheric temperatures, has been described by [?] and [Ribes et al., 2009]. Considering the stratospheric temperatures show a seasonal pattern, an elementary trend model for describing stratospheric temperatures can be written as:

$$\hat{y}_t = \mu + S_t + \alpha X_t + \epsilon_t$$

Here, $\hat{y}$ is the estimated value of the dependent variable, temperature. μ is a mean or constant value around which the temperature oscillates. S_t is a seasonal component, approximated by [?] in the following manner: $\sum_j^4 \beta_{1,j} sin(\frac{2\pi jt}{12}) + \beta_{2,j} cos(\frac{2\pi jt}{12})$. The term αX_t describes a linear trend that is being sought. α is the trend coefficient per year which is multiplied by $X = \frac{1}{12t}$, since the input data are monthly means. The ϵ represents a autoregressive noise process.

This elementary trend model can be extended with components that contribute to the temperature within the stratosphere. As was discussed in chapter 2, the temperature is mainly determined by its chemical constituents, radiative properties and dynamical processes. Ozone and carbon dioxide are the dominant species in determining the radiative balance of the stratosphere. According to combined satellite and ground measurements, O_3 depletion has been flattening off since the late 90's, and has shown onset of recovery in the last decade [Ajavon et al., 2018]. Along with the decreasing ozone depletion, the ozone induced cooling trend is presumed to have decreased as well. Simultaneously, CO_2 abundance has increased, leading to cooling, most prominent in the middle and upper stratosphere. To distinguish between the ozone and CO_2 signals, only ozone concentrations are added to the trend model. Ozone concentrations are measured at the same measurement site, thus representative ozone data is available. The left panel of figure 3.2 shows the ozone column data. Ozone column is given in Dobson Units, one DU equals 10 μm of pure ozone when compressed to surface pressure. The ozone column shows a seasonal trend, peak values of ozone column correlate different with temperature throughout the stratosphere. In the low to middle atmosphere, temperature and ozone concentrations are in phase and do correlate well. In the upper stratosphere, temperatures lag behind ozone peaks and troughs, the correlation is thus weaker. The right panel of figure 3.2 shows an ozone profile for ozone number densities at October 1998. The ozone layer is recognizable at 25 kilometres. The ozone column is fairly constant but shows slight increases in the final decade of the timeseries. For the 1995-2017 timeseries, a increase of 0.2% per decade is estimated for the ozone column.

timeseries/ozonecolumndata.png timeseries/O3profileexample.png

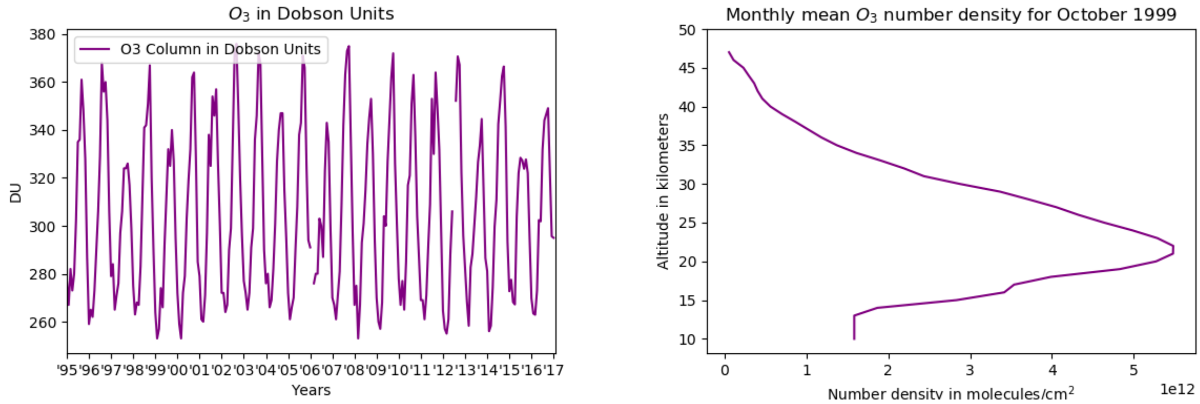

Figure 3.2: *Left panel: Ozone Column data in Dobson Units (DU) Right panel: Monthly mean ozone profile for October 1998, measured by the Lauder Lidar.*

An important process in determining the irradiance in the stratosphere is the 11-year solar cycle. This cycle creates additional variability in the available solar energy in the stratosphere for ozone absorption and heating of the troposphere, which in turn will radiate to the stratosphere. The solar cycle is approximated using the 10.7 cm radio flux. This flux of radio-waves is a long running continuous dataset on solar activity. The radio flux is considered a valuable, robust dataset (NOAA). The 10.7 cm radio flux available from the World Ozone and Ultraviolet Radiation Data Centre (WOUDC) and is portrayed in the left panel of figure **??**. The Lauder timeseries span a period which consists of two solar cycles, the first one being stronger than the second.

Dynamical aspects in the stratosphere include the Brewer-Dobson Circulation (see section 2.1.2). The brewer dobson circulation is difficult to quantify directly. After [Visser and Molenaar, 1995], the Quasi Biennial Oscillation is taken as a temperature proxy. The QBO interferes with the brewer dobson circulation, the oscillation of zonals winds is simulated via a proxy, the strength of 10 hPa level, near equatorial zonalwinds. This proxy was taken from [de Winter-Sorkina, 1995] and [Steinbrecht et al., 2009] . The QBO winds are connected to the temperatures via a constant and a phase lag. The right panel of figure **??** shows the oscillation.

timeseries/Radioflux.png timeseries/QBOproxy.png

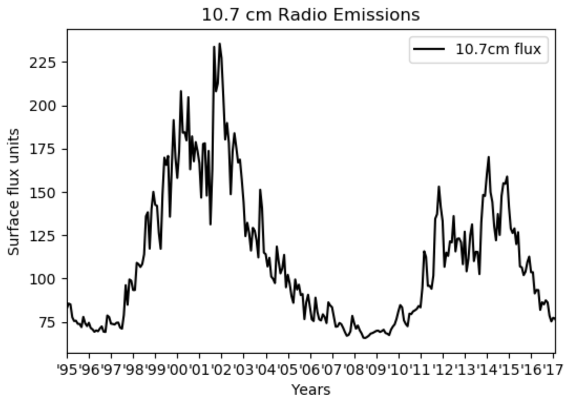

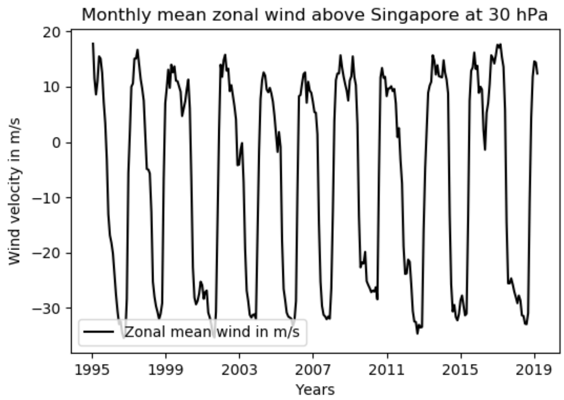

Figure 3.3: *Right panel: 10.7 cm Radio flux data. Data taken from the NOAA and WOUDC. Left panel: Quasi-biennial oscillation. Winds turn from westerly to easterly with time periods of about 26 months [de Winter-Sorkina, 1995].*

When the ozone column, solar cycle and QBO are added to the trend model, the model is extended to:

$$\hat{y_t} = \mu + S_t + \beta_{o_{3},j} * [O_{3j}] + \beta_{sun} * [F] + \beta_{qbo} * QBO + \alpha X_t + \epsilon_t$$

Here, the β 's represent constants which connect the corresponding variable to the temperature. The ozone constant and seasonal value is dependent on the month. The equation is solved using the observed data as input and estimating the best fit using a least square method. The estimated trend is then interpreted as a factor which will, at least to some extend be assigned to warming due to CO_2 increase. Although this trend model is expected to include a large part of the variation in the stratospheric temperatures, it does not cover all effects. An explicit description of the Brewer Dobson strength is lacking and also additional chemical constituents like H_2O, and aerosol effects are missing. Additionally, the longwave emission, cooling effect, of ozone might interfere with the assignment of a trend to the ozone increase. A direct conversion from the trend to CO_2 might thus be difficult to find. However, to a good extent, the trend is expected to be dominated by CO_2 increase. The O_3 component to the temperature trend in the stratosphere can than be calculated by performing the regression on the temperature estimation, solely based on the ozone part of the trend model, with the corresponding constants found for the specific altitude layer. Analysis is initially done for four parts of the stratosphere:

1) Lower stratosphere: 15-25 kilometres
2) Middle stratosphere I: 20-30 kilometres
3) Middle stratosphere II: 30-40 kilometres
4) Upper stratosphere: 40-50 kilometres

The lower stratosphere altitude range corresponds to the MSU Channel for satellite temperature measurements. The middle stratosphere altitude ranges are chosen such that they lie just within and above the part where ozone abundance is highest. The altitude bins correspond roughly with the altitude ranges used in the analysis done in previous studies [Maycock, 2016b][Maycock et al., 2018][Seidel et al., 2011][Mitchell, 2016]

4 Results

This chapter presents the results that were found in the analysis of the temperature profiles. The trend model used is discussed before starting of with the Lauder profile results. After Lauder, the other temperature profiles that were analysed are discussed. The chapter will close with CMIP5 predictions of stratospheric temperatures.

The Lauder temperature profile data, derived by Anne van Gijsel, has been analysed using Python. The raw data has been filtered for extremely low and high values ($170K < T > 300K$). These values occur several times in the measurements but are unreasonable for the stratosphere and are thus regarded as incorrect. Figure 4.1 shows the Lauder data for different altitudes. Quick visual inspection shows a seasonal temperature spread that becomes larger when propagating upward. Around the tropopause level, the data contains multiple outliers of low temperatures, up to 180K.

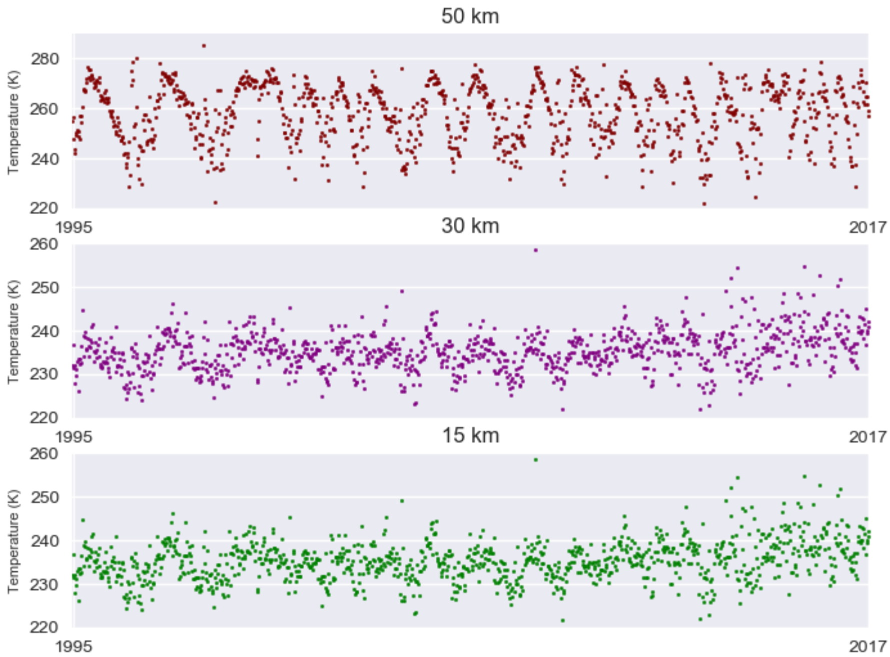

Figure 4.1: *Raw data of the Lidar temperature data for the stratosphere at different altitudes. Altitude ranges around the given altitude are +/- 500 metre. Data are retrieved for the period 1995-2017. Temperature ranges from 285-220 K around the stratopause to 250-180 K around the tropopause.*

A complete image of the data is portrayed in Figure 4.2. The vertical temperature structure of the stratosphere is easily distinguishable. The larger seasonal variability in the upper stratosphere cause the vertical temperature gradient to be smaller during winter than in summer. The figure also shows that the timeseries is almost continuous up to 2008. The data gap around 2008 is a remarkable feature, due to changes and maintenance on the Lidar. After 2008, measurements become less frequent. This is partially caused by adjustments in measurement strategy between 2011 and 2014 that were undertaken.

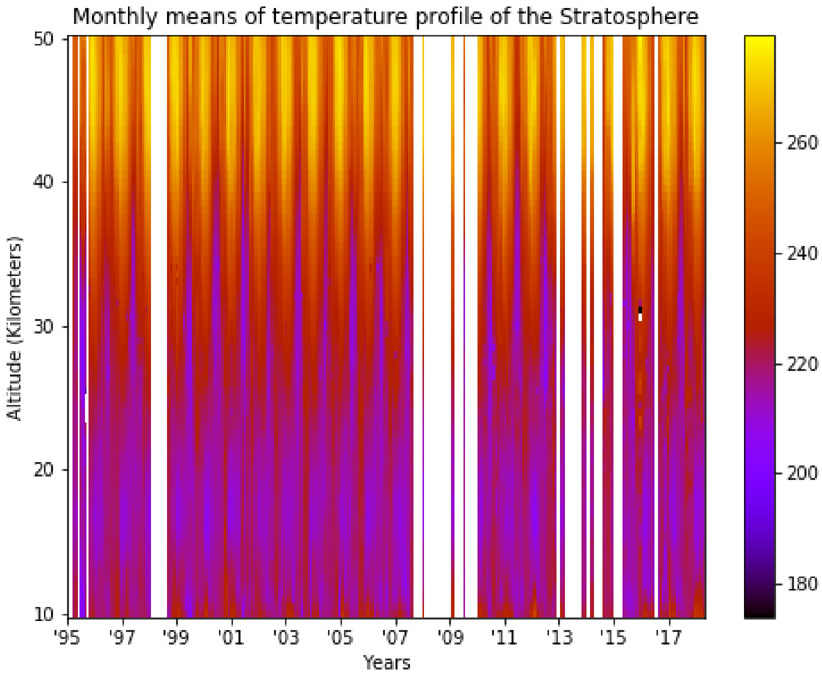

Figure 4.2: *Monthly mean temperatures from 10-50 kilometres altitude, measured by the Lauder Lidar. Vertical resolution is 500 meters. Averages are taken +/- 500 m around given altitude.*

An example of the different components of the trend model is shown in figure 4.3. The residuals are interpreted to be a combination of ϵ_t and the trend α. The trend is given with a uncertainty range, the corresponding two tailed p-value and the sum of squared residuals (SSR). From figure 4.3 it becomes clear that the seasonal and ozone components are dominant in determining the temperature. Addition of the solar cycle and especially the QBO adds very little to goodness of the trend estimation. Figure 4.3 shows that an overall positive trend is found for the lower stratosphere. The trend is about 0.18 K/dec but has a relatively large standard deviation of +/- 0.15 K/dec.

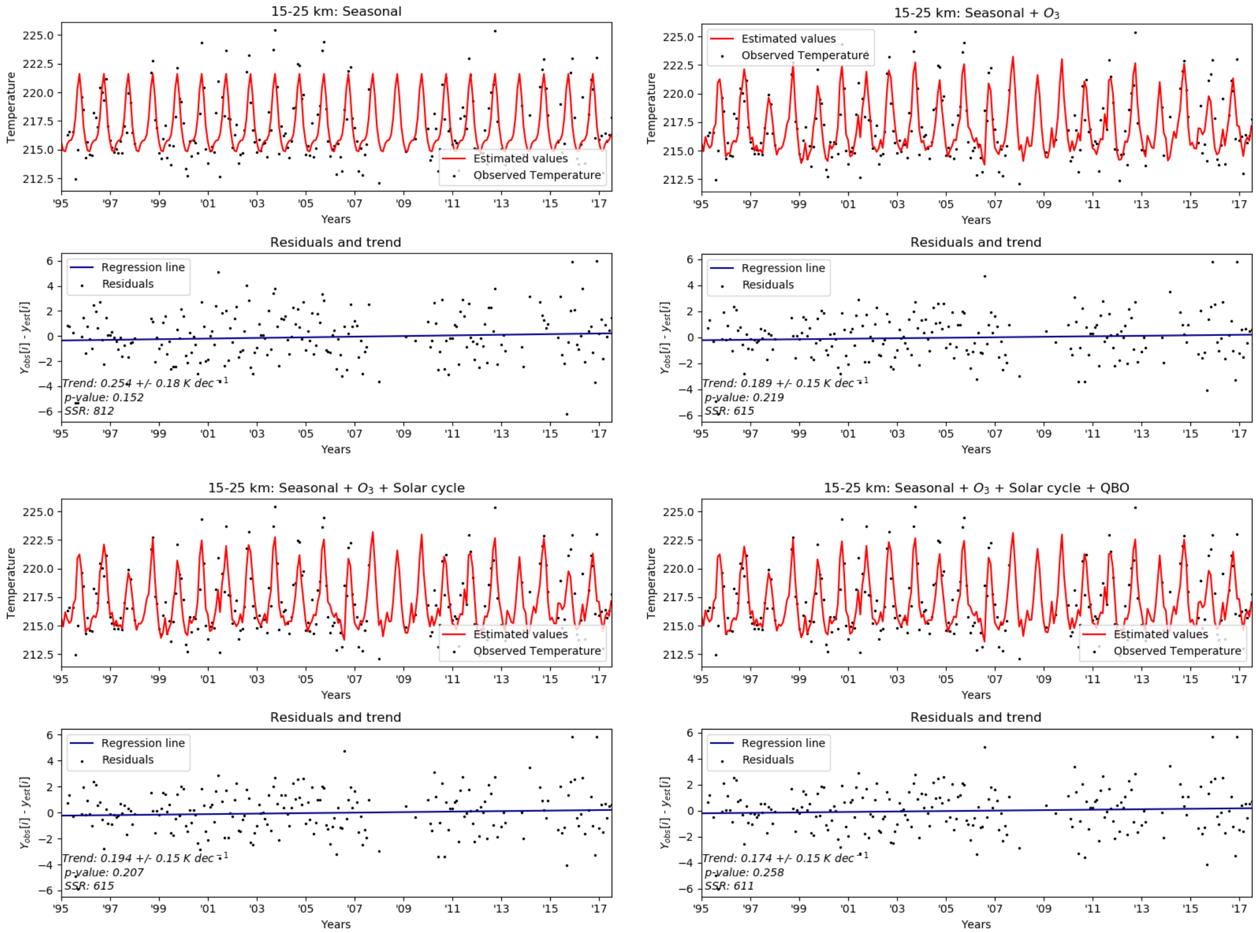

Figure 4.3: *Estimated values for the trend model are shown compared to the observed values, for the lower stratosphere altitude bin. Starting with the Seasonal cycle, the estimations consecutively superposition the Ozone column, Solar radiation fluctuations and the QBO-oscillation. The upper curves, in red show the estimations of the trend model. The lower graphs show the residuals and the trend line, in blue. Confidence intervals given as 1 σ.*

4.1 Lauder timeseries

Table 4.1 shows the outcomes for the complete time period. The middle stratosphere bins holds negative temperature trends. The first bin, located around the ozone layer, has a magnitude of -0.31 ± 0.22 and is significant on the 85% confidence interval. This trend does agree with literature. Other trends are relatively uncertain. For the upper and lower stratosphere, positive trends are found.

Table 4.1: *Trend values for 1995-2017 estimated from monthly mean temperatures. Positive are detected in the upper and lower stratosphere. Negative trends in the middle stratosphere. The only significant trend (on 85% confidence interval) is a negative trend between 20-30 kilometres.*

'95-'17	**Altitude (km)**	**Trend (K/dec)**	**P-value**
Complete estimation	15-25	0.14 ±0.17	0.40
	20-30	-0.31 ±0.22	0.15
	30-40	-0.06 ±0.43	0.89
	40-50	0.45 ±0.52	0.38

Table 4.2 shows the trend model analysis for the period spanning 1995-2007. In the lower stratosphere, up to 30 kilometres, positive trends are found. Negative trends are detected by the trend model for higher altitudes. The upper stratosphere trend is -1.9 ± K/dec, this is on the high end of estimates by previous studies [Maycock, 2016b] (-0.6 ± 0.02 K/dec greenhouse gas induced and -1.3 K/dec including all drivers) and [Maycock et al., 2018] (-0.8 ± 0.4 K/dec including all drivers). The middle stratosphere I contains a trend with large uncertainty of 0.3 ± 0.82. For these altitudes, [Maycock, 2016b] finds -0.5 ± 0.02 due to greenhouse gasses, [Maycock et al., 2018] finds 0.5 ± 0.9 K/dec including all drivers. The MSU1 and SSU1 (15-25 and 20-30 km) altitudes show positive values with large confidence intervals. These values do not agree with mentioned studies. Confidence intervals are large, meaning that the found trend is not very robust.

Table 4.2: *Trend analysis values for the first time period, spanning 1995 - 2007 estimated for monthly mean temperatures. The complete estimation is shown, meaning all terms explained in section 4.1.1 are used as model input.*

'95-'07	**Altitude (km)**	**Trend (K/dec)**	**P-value**
Complete estimation	15-25	0.33 ±0.40	0.41
	20-30	0.18 ±0.55	0.73
	30-40	-.30 ±0.22	0.51
	40-50	-1.9 ±0.90	0.04

Table 4.3 shows the trend analysis results for the time period 2005-2017. For this period all altitude bins except for the middle stratosphere II contain positive trends. However, the trends are highly uncertain. As mentioned, the observational timeseries in this periods has a lot of gaps, additionally, changes in measurement strategies were started in 2011 and a new laser was installed in 2008. These adaptation reflect in the uncertainty values and the apparent warming of the stratosphere. A net warming in the upper stratosphere as is visible in the table is theoretically not a realistic outcome. The fingerprint associated with CO_2 is expected to be strongest in the upper stratosphere. Additionally, the trend estimations in the highest

two altitude bins suffer from extremely high uncertainty, compared to the magnitude of the detected trends. Whether the trends found in the second time period are due due to errors in the model, improper calibration of the temperature data for the adjustments or due to an existing process in the stratosphere is discussed later.

Table 4.3: *Trend values for 2005-2017 estimated from monthly mean temperatures. The trend model finds dominantly positive trends for this time period. This period is marked by gaps in the dataset and changes in measurement strategies. This causes the dataset to be less reliable from 2010 onwards.*

'05-'17	**Altitude (km)**	**Trend (K/dec)**	**P-value**
Complete estimation	15-25	0.0 ±0.42	0.98
	20-30	-0.78 ±0.50	0.11
	30-40	0.05 ±1.11	0.96
	40-50	0.09 ±1.40	0.42

From the previous tables it becomes clear that the trend model has problems detecting significant trends in the Lauder temperature profiles. Partially this may be due to measurement and calibration errors. Especially the second period is prone to biasses in the trend model due to the discontinuity of the measurements and changes in measurement strategy. For the early time period, stratospheric temperature trends found in previous work do agree on the trends that are detected in the Lauder timeseries. [Maycock et al., 2018] analysed the AMSU and SSU satellite data for the time period 1979 to 2016. In contrast to the Lauder dataset, they find negative trends throughout the complete stratosphere. However, the found trends of -1.0 ± 0.5 and -0.6 K/dec ± 0.5 K/dec for the SSU2 and SSU3 (35-45 and 40-50 km) channels between 1979 and 1998 are in between the Lauder trends for 1995-2007. [Seidel et al., 2011] also revisions the SSU and AMSU temperature data and finds weaker negative temperature trends. For the middle and lower stratosphere, the positive temperature trends found in the early time periods are uncertain but could be explained by the fact that it is yet unsure at which altitude greenhouse gas induced cooling takes over from warming., Different papers argue that the lower stratosphere is just around this tipping point [Randel et al., 2009] [Maycock, 2016a]. Additionally, the temperature in the lower stratosphere is more strongly influenced by tropospheric processes and containts more high frequency variations.

EOF and SVD analysis

The analysis in the previous section was done on monthly averaged and linearly interpolated values of the raw data. In this case, the model only found significant trends ($p < 0.15$) for the early time period in the upper altitude bin and for the complete time period in the middle stratosphere I altitude bin. To reduce the noise signal in the dataset, an Empirical Orthogonal Function (EOF) method is performed on the timeseries. Additionally, Singular Value Decomposition (SVD) is done to gain a more insight in the covariance of different variables, this might lead to a better understanding of the different processes that are important at different altitudes within the Lauder profiles.

The EOF method used is taken from Björnsson & Venegas, (1997). The method involves the construction of an auto-covariance matrix of data within the altitude bins. Solving the eigenvalue problem for this covariance matrix gives an eigenvector matrix containing n eigenvectors, in which n equals the amount of timeseries that are involved. Each eigenvector is a temporal pattern which explains a fraction of the variance in the temperature. The fraction explained is given by the corresponding eigenvalue. By only projecting the eigenvectors with the largest eigenvalues, the temperature series can be 'reconstructed' to a temperature series that is reduced in its noise signal.

Lauder 40-50 km

Figure 4.4 shows the results of the trend model run on the reconstructed timeseries. The timeseries shown is reconstructed with the first four eigenvectors. The uncertainty is clearly reduced, however, the trend model still fails to adequately capture outliers, especially to the colder temperatures. For the 1995-2007 time period, a trend of -1.46 ± 0.53 K/dec is detected. From 2005-2017, a positive trend is found of 0.37 ± 0.16.

The ozone contribution can be derived by only calculating the temperature, influenced by the ozone column, as estimated by the trend model. In this way, the ozone trend is found to be negligible for the first time period and has a warming contribution to the Lauder timeseries of approximately 0.15 K/dec.

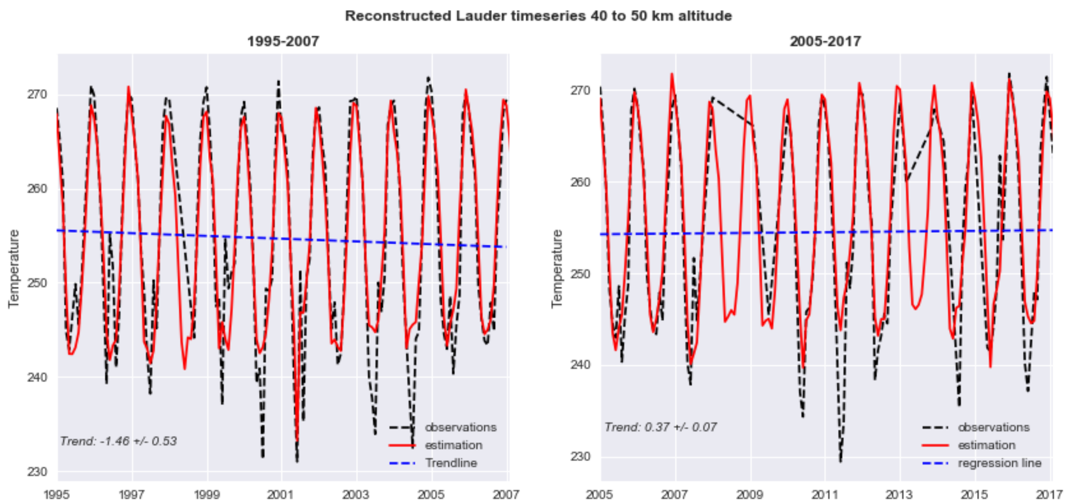

Figure 4.4: *Trend model run on the reconstructed timeseries. The reconstruction is derived from the four leading terms of the Empirical Orthogonal Function method [Bjornsson. and Venegas., 1997]. Uncertainty values are given at one standard deviation of the estimated trend. The left panel shows the 1995-2007 time period, the right panel the 2005-2017 time period.*

The Singular Value Decomposition method [Bjornsson. and Venegas., 1997] shows the covariance between timeseries of different variables. Variables used for the SVD method are ozoneconcentration, temperature and solar activity. The method is similar to the EOF method, however, the use of multiple variables to generate one covariance matrix results in one eigenvector per variable. Every component of an eigenvector now represents the correlation of the eigenvector to the corresponding variable. By reviewing the responses of different variables to an eigenvector, an underlying mode of variation can be deduced. However, since the SVD is merely a mathematical method, care has to be taken in appointing a physical process to a specific mode.

The results for the SVD on the timeseries of ozone, carbon dioxide, solar cycle and the stratospheric temperature is shown in table 4.4. The first eigenvector projects in opposite sign to temperature and CO_2 and very weak on O_3. The strong projection on both temperature and CO_2 indicate that this mode is associated with temperature variability, driven by increase in atmospheric CO_2 burden. The eigenvalue of this eigenvector is large, pointing to the dominance of the CO_2 signal in determining temperature trends in the upper stratosphere. The weak correlation with ozone can be explained by negative feedback of stratospheric cooling on ozone. This feedback is caused by decreasing reaction rates of ozone depleting substances, slowing ozone destruction [Lacis and Hansen, 1973][Maycock, 2016a]. The second eigenvector explains 20

Table 4.4: *Eigenvectors given for the altitude bin 40-50 kilometres. The variables have been deseasonalised before the SVD method was performed. Eigenvectors calculated for the complete time period (1995-2017).*

	λ_1	λ_2	λ_3	λ_4
Temperature	0.71	0.05	0.13	-0.68
Ozone	-0.06	-0.63	-0.72	-0.25
CO2	-0.61	-0.25	0.48	-0.57
Solar	-0.32	0.72	-0.47	- 0.37
Eig.value	0.61	0.20	0.17	0.02

Lauder 30-40 km

Figure 4.5 shows the EOF based reconstructed timeseries for the SSU2 altitude bin. Similar as in the SSU3 altitude bin, the early time period does inhibit a greenhouse gas trend of about -0.40 ± 0.33 K/dec whereas from 2005-2017 no significant trend is detected. Uncertainty for the 2005-2017 trend is higher than the trend value, which is practically zero. Contributions of ozone is estimated at +0.1 K/dec for the 2005-2017 time period and negligible until 2005.

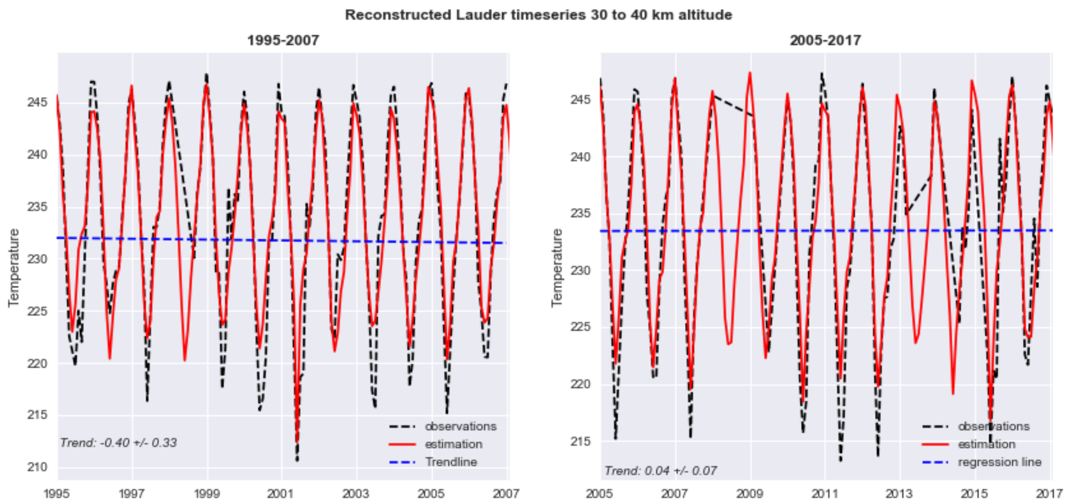

Figure 4.5: *Same as figure 4.4, but for the 30-40 km*

Results of the SVD for this altitude bin are portrayed in table 4.5. The eigenvectors and values are similar to the eigenvectors derived in the upper stratosphere. However, the assumed CO_2 mode corresponds to the second eigenvector, indicating this mode is less important in explaining variance between the variables. The projection on temperature is nevertheless strong. The projection of the first eigenvector is comparable in magnitude for all variables. However, the projection is positive for temperature and CO_2 and negative for O_3 and the solar flux. An interpretation of this mode is not given. The third eigenvector projects strongly on ozone and is interpreted in the same way as in the upper stratosphere: ozone column fluctuation.

Table 4.5: *Same as table 4.4 but for the 30-40 km altitude bin.*

	λ_1	λ_2	λ_3	λ_4
Temperature	-0.49	-0.66	-0.15	-0.52
Ozone	0.45	-0.17	0.75	-0.43
CO2	-0.45	0.71	0.13	-0.51
Solar	0.58	0.11	-0.62	-0.51
Eig.value	0.52	0.27	0.20	0.01

Lauder 20-30 km

The reconstructed timeseries for the SSU1 altitude bin are portrayed in figure 4.6. Similar as in the first trend model run, the 1995-2007 time period contains a uncertain trend of +0.18 ± 0.22 K/dec whereas from 2005-2017 a negative trend of -0.86 ± 0.07 K/dec is detected. Uncertainty margins are reduced and trend values are larger compared to the first trend model run. In comparison with the higher stratospheric layers, the sign of trends is reversed for both time periods. The effect of ozone on the trend is negligible from 1995-2007 and 0.1 K/dec ± 0.04 K/dec from 2005-2017.

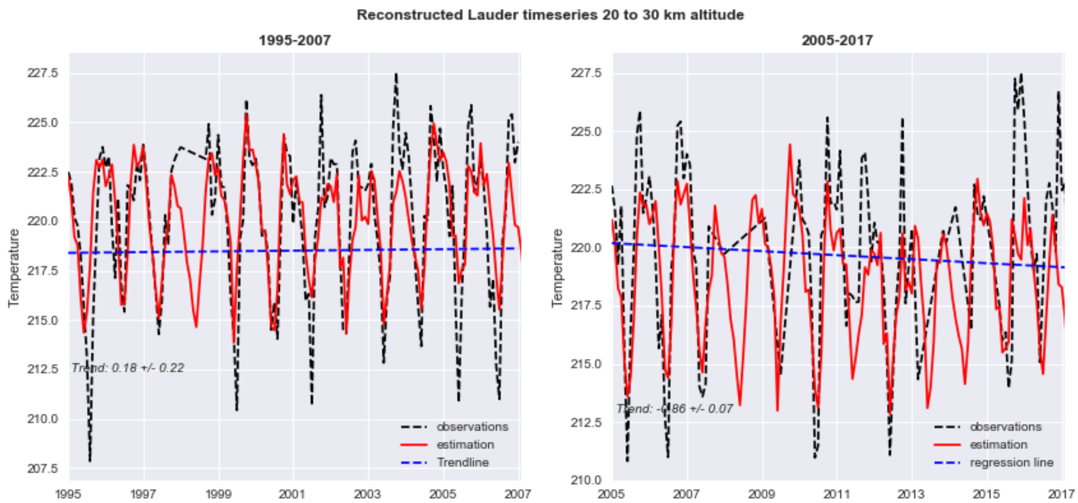

Figure 4.6: *Same as figure 4.4, but for the 20-30 km altitude bin.*

The first eigenvector projects particularly strong on CO_2 and in opposite direction on temperature and ozone. The projection on ozone is weak. This eigenvector is again associated with

CO_2 increase, indicating that atmospheric greenhouse gas concentrations still impose a negative temperature trend in this part of the stratosphere. The second eigenvector projects strongly on temperature and moderately on ozone. A process to understand this mode of variance is difficult to give. The strong projection on temperature combined with its anticorrelation with the other variables can not be comprehended by physical processes. The third eigenvector projects strongly on ozone and moderately on temperature. Therefore this eigenvector is associated to project the ozone variance. Although the second eigenvalue is not clarified, from the SVD it can be concluded that also in this part of the stratosphere, CO_2 influences dominate ozone contributions to a temperature trend.

Table 4.6: *Same as table 4.4 but for the 20-30 km altitude bin.*

	λ_1	λ_2	λ_3	λ_4
Temperature	-0.24	0.83	-0.18	-0.45
Ozone	-0.37	-0.49	-0.64	-0.44
CO2	0.77	-0.10	0.06	-0.62
Solar	-0.45	-0.21	0.73	-0.45
Eig.value	0.48	0.28	0.23	0.01

Lauder 15-25 km

For the AMSU/MSU altitude bin, temperature trends for both time periods are positive, with trend values of respectively 0.49 ± 0.22 and 0.41 ± 0.13 K/dec. High frequency variability is large compared to other altitude bins. This can be an explanation for the relatively high uncertainty margins of the trends. Again, the ozone trend on the temperature series is effectively zero for the first time period and 0.1 ± 0.12 K/dec for 2005-2017.

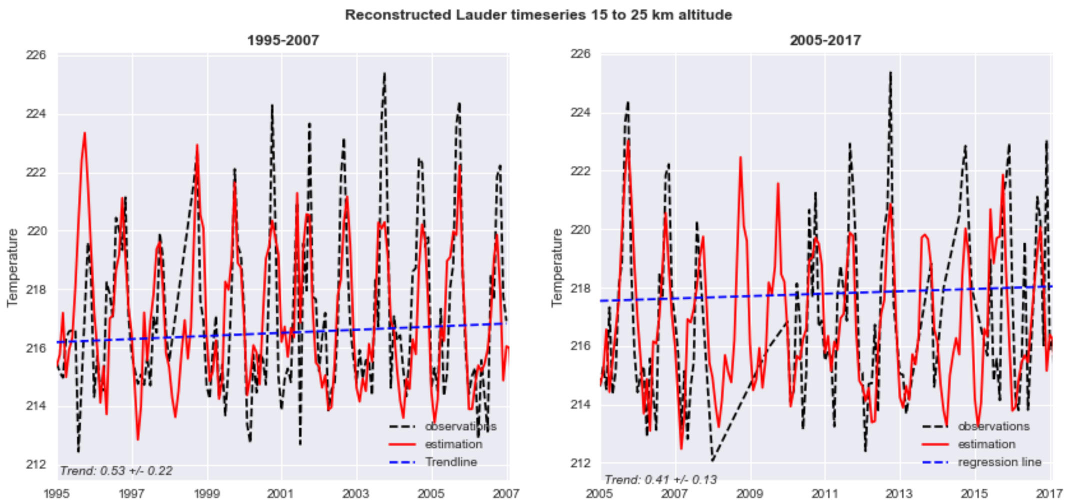

Figure 4.7: *Same as figure 4.4, but for the MSU/AMSU altitude bin*

Table 4.7 shows the eigenvectors for the 15-25 kilometre altitude bin, the projections of the different eigenvectors are equal as those for the 20-30 altitude bin, also the magnitudes of the components are very similar. The modes are thus interpreted the same.

Table 4.7: *Same as table 4.4 but for the 15-25 km altitude bin*

	λ_1	λ_2	λ_3	λ_4
Temperature	-0.40	-0.36	0.81	0.19
Ozone	-0.14	- 0.72	-0.50	0.44
CO2	0.73	0.06	0.24	0.63
Solar	-0.52	0.58	-0.14	0.60
Eig.value	0.53	0.38	0.08	0.01

To conclude the Lauder data analysis, the Lauder temperature profiles do contain temperature trends. With dimensional reduction to increase the signal/noise ratio, the early time period contains negative trends for the stratosphere above 30 kilometres. These trends are significant on a 90% confidence level. The discovered trends are -1.4 and -1.9 K/dec. These trends are higher than temperature trends in other papers [Maycock et al., 2018][Maycock, 2016b][Mitchell, 2016], which could point to a strong contribution of CO_2 or other signals that are at play but not accounted for in the trend model. In the two highest altitude bins, the trends are obscured in the longer time periods, due to apparent warming in the second part of the timeseries. Below 30 kilometres, trends become slightly positive with relatively high uncertainty levels. Due to the high uncertainty, between 20-30 kilometres, the sign of the temperature tendency might as well be opposite than found by the trend model. For the later time period, the stratosphere contains a significant trend of -0.86 K/dec between 20 and 30 kilometres. For the other altitudes, detected trends are small, positive and with high uncertainty.
It was found that the changes in ozone column above Lauder induce no net trend over the years 1995-2007. The trend from 2005-2017 ranged from 0.1 ± 0.05 K/dec, slightly higher than the global mean values found by [Maycock, 2016b] of 0.07 ± -.05 K/dec. Ozone trends are very similar throughout the altitude bins.

4.2 Comparison with other datasets

In the previous sections we came to the conclusion that the Lauder dataset does contain temperature trends. However, these are not uniform for the complete timeseries. Several explanations can be given for discrepancy between the early and later time period. First, an explanation can be found in the experimental setup of the Lidar. A new ozone measurement method was implemented from 2011 onwards. This has not yet been calibrated well, which also reflects in the local ozone values derived from the Lidar for the same period (van Gijsel, personal contact). Furthermore, the timeseries contains several periods of missing data, varying from several months to almost a year without measurements. The largest data gaps are found in 1998, and between 2008 and 2014. Second, it is possible that the temperature in the stratosphere above Lauder does not respond as strongly as expected at certain layers or at specific timeperiods. This means that the Lauder temperature profiles do not at all altitude levels agree with the temperature trends that were found in the SSU and AMSU data [Maycock et al., 2018][Maycock, 2016b][Mitchell, 2016]. A paper by [Ferraro et al., 2015] proposes the possibility of a hiatus in the cooling of the stratosphere, This halt in stratospheric cooling started in the early 00's. [Ferraro et al., 2015] argues this stratospheric temperature hiatus to be an analogue of the warming hiatus which is recognized for global sea surface temperatures and is the result of internal variability and/or redistribution of heat in the climate system. Finally, the trend model does not capture all variability present. This means the found trends can not be assigned to CO_2 only. Other effects as increasing ozone cooling or changes in dynamics can also cause temperature shifts.

In order to get a better understanding in the results of the Lauder temperature profiles. The Lauder data is compared with other stratospheric temperature datasets. Unfortunately, the NDACC does not have a wide range of Lidar measurements available. Also, the spatial distribution of measurements in the southern hemisphere is poor. Therefore three different sonde measurements and one Lidar temperature timeseries are used for comparison with the Lauder data. The sonde timeseries are taken from Dumont d'Urville, Neumayer and Boulder. The first two stations are located at Antartica. The third is at Boulder, US. The latitudinal location of Boulder in the Northern Hemisphere is comparable to Lauder. The sonde measurements extend until roughly 30 kilometres altitude and thus only allow for comparison with the lower part of the Lauder dataset. The Lidar timeseries is taken from Stromfjord, Greenland. These Lidar measurements start from 30 kilometres and run up until 80 kilometres.

Table 4.8: *NDACC observation stations used in the analysis*

Station name	**Location**	**Measurement**
Dumont d'Urville, Ant	66.67°S, 140.00°E	Sonde
Neumayer, Ant	70.62°S, 8.37°E	Sonde
Boulder, US	39.99°N, 105.26°W	Sonde
Stromfjord, Grld	66.99°N, 50.95°W	Lidar
Lauder, NZ	45.04°S, 169.68°W	Lidar

For all the timeseries, the input for the Solar cycle and QBO-oscillation in the trend model are the same as the Lauder timeseries. The ozone profiles are locally measured profiles taken from the World Ozone and Ultraviolate Radiation Data Centre. The ozone values for the different observational stations are portrayed in **??**. The Boulder ozone column change is a bit higher than the Lauder change: 0.8 ± 0.49 %/dec with respect to the average ozone column for the 1995-2000 time period. The Antarctic and Greenland ozone column values show larger increase and have lower uncertainty. Antarctic column changes are estimated at 2.43 ± 0.93 %/dec, Greenland changes are estimated at 2.21 ± 1.28 %/dec. For the stations situated at higher latitudes it is visible that the ozone recovery shows seasonal dependence, with highest recovery rates in the spring time.

timeseries/ozoneanomalies.png

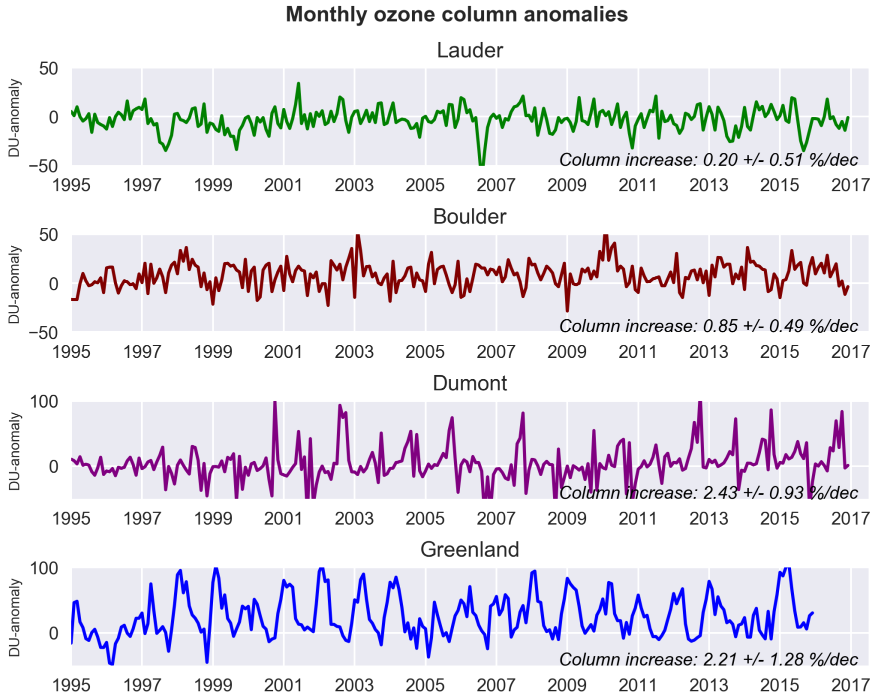

Figure 4.8: *Ozone anomalies in DU. Anomalies with respect to the 1995-2000 time period monthly means. Mind the different scales for the Dumont and Greenland timeseries, here ozone anomalies are significantly larger than for the Lauder and Dumont timeseries.*

Dumont d'Urville

A reconstructed version of the Dumont timeseries and the corresponding interpreted greenhouse gas trend is portrayed in figure 4.9. The reconstructed timeseries involves the four leading modes of variance. The trend model is used again to estimate the trends. In the 20-30 kilometre range (upper panel of figure **??** the estimated trends are negative: -1.77 ± 0.64 K/dec temperature change for 1995-2007 and -1.44 ± 0.38 K/dec for 2005-2017. The 15-25 kilometre altitude bin (lower panel of figure 4.9) contains a uncertain trend, both in sign and magnitude for the first time period. For 2005-2017, the trend is strongly negative: -2.22 ± 0.52 K/dec. The ozonelayer altitude bin thus shows a continuous trend throughout the timeseries, whereas in the lower stratosphere, a trend has emerged during the 00's. For the complete timeperiod the trend assumed to be CO_2 induced equals 1.49 ± 0.25 K/dec.

From 1995-2017, the Antarctic ozone column, measured above Dumont d'Urville increased with an average of 2.3% per decade. This is clearly reflected in the trend induced by ozone. The 1995-2017 ozone induced trend is estimated at +0.26 ± 0.13 K/dec. However, measured from 2005-2017, the O_3 signal becomes stronger: +0.66 ± 0.27 K/dec. The contribution of ozone is thus strongly positive for the later part of the temperature series in Dumont. The ozone signal is nearly equal for both altitude bins. Greenhouse gasses, ozone and solar fluxes combined give a net stratospheric temperature trend of approximately 1.3 and 0.5 K/dec.

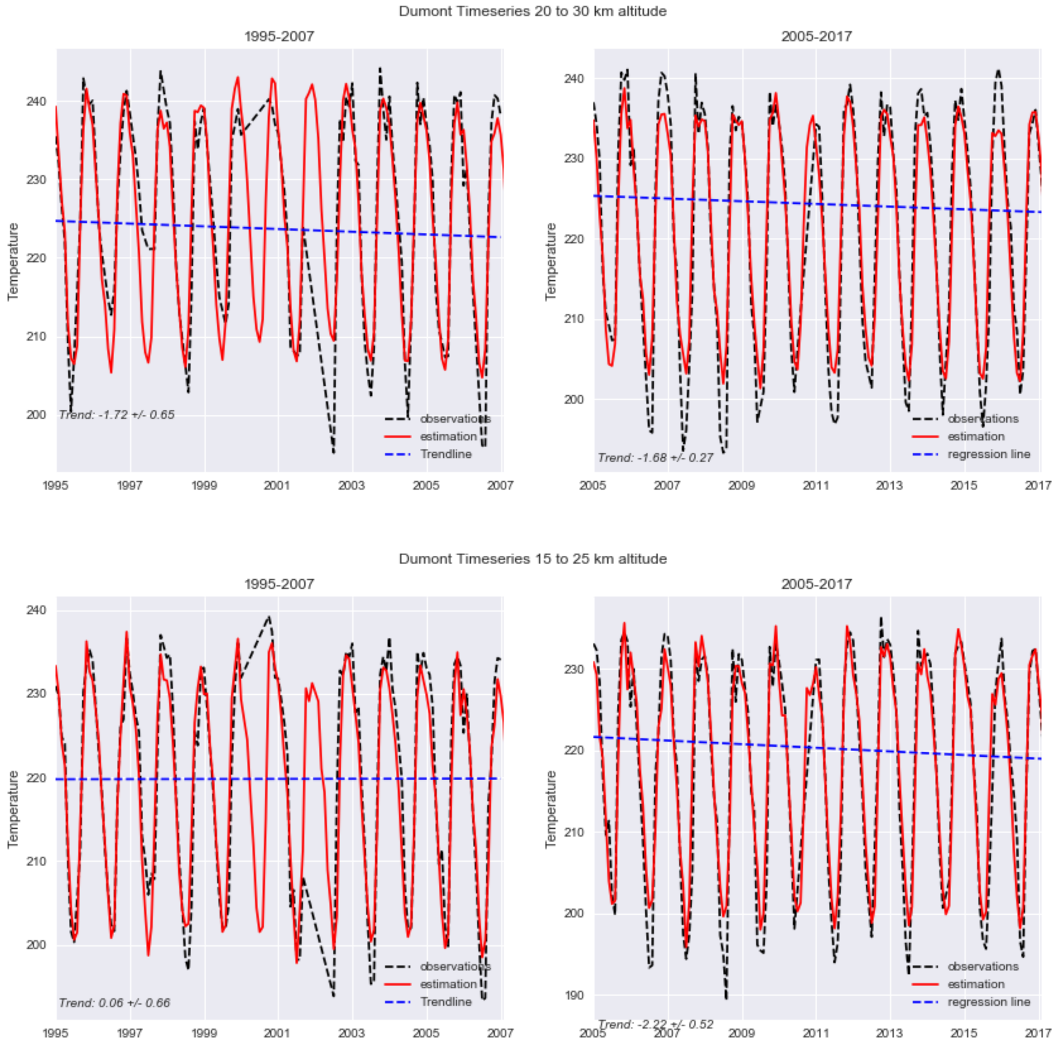

Figure 4.9: *Same as figure* **??** *but for Dumont d'Urville station for 20 to 30 kilometres altitude.*

Detected trends in Dumont are thus much stronger than those found in Lauder. The Dumont timeseries is characterised by an observational record that is regular and complete. Furthermore, the ozone column values for Dumont show the strongest increase in ozone concentration of all observations.

Table 4.9 shows the eigenvectors for a Singular Value Decomposition performed on the timeseries of different drivers in the stratosphere. The first eigenvector is associated with increase in greenhouse gasses. The anticorrelation of temperature and CO_2 and the weak correlation with ozone makes this a plausible process for the variance explained by this mode. The second mode of variance also projects strongly on ozone and moderately on both temperature and the solar flux. Solar fluctuation can explain the strong projection on ozone, however, the anticorrelation with temperature can not be explained then. The third eigenvector projects strong on ozone and in equal direction on temperature, projection on CO_2 is the opposite. Therefore it seems that this eigenvector represents the ozone column or ozone concentration, responsible for warming in the stratosphere. The first mode dominates the variance in the different variables. This makes it plausible that CO_2 is the dominant component in determining the stratospheric temperature trend. The second mode, with its projection dominantly on the solar cycle, explains a smaller portion whereas ozone is the smallest of three components to influence the temperature trend.

Table 4.9: *SVD eigenvectors (λ) of the Dumont timeseries, showing the correlation of different processes on Temperature, O_3, CO_2 and the incoming Solar flux. Eigenvectors for the period 1995-2017.*

	λ_1	λ_2	λ_3	λ_4
Temperature	-0.61	-0.42	0.24	0.61
Ozone	0.25	0.32	0.90	0.12
CO2	0.68	-0.14	-0.23	0.67
Solar	-0.30	0.82	-0.26	0.38
Eig.value	0.67	0.20	0.11	0.02

Neumayer

Figure 4.10 shows the timeseries taken from the Neumayer station, Antarctica. The Neumayer station lacks accurate ozone measurements, therefore the ozonecolumn from Dumont d'Urville is taken as input for the trend model. Additionally, the Neumayer timeseries has a significant amount of gaps in the dataset, especially in the winter months. The timeseries is characterised by positive trends in the time period of 1995-2007: corresponding trends for the 20-30 and 15-25 km altitude bins are $+1.70 \pm 0.33$ K/dec and $+0.09 \pm 0.66$ K/dec. Here, uncertainty in the lower stratosphere is high, which was also the case for the Dumont timeseries. It is unclear how to interpret the 1995-2007 temperature trend. Although greenhouse gasses might induce a minor positive trend in the lower stratosphere, large magnitudes like these are at odds with current understandings. The trend line of the timeseries for the complete timeperiod is negative. This is due to the negative trends in the second part of the timeseries. The years 2005-2017 are characterised by negative trends: -1.21 ± 0.25 K/dec and -2.23 ± 0.57 K/dec for the 20-30 and 15-25 km altitude bins. Similar to the Dumont timeseries, the trend in the lower stratosphere is larger than in the middle stratosphere. The net negative trend for 1995-2017 does agree fairly well with [Seidel et al., 2011][Maycock, 2016b]. The individually found negative trends on the high end of previous estimations, although overall, antarctic temperature trends are stronger than global trends [Maycock et al., 2018]. The net CO_2 induced temperature trend is found to be -1.60 ± 0.67 K/dec for the 15-25 altitude range. For the 20-30 kilometre altitude bin, the 1995-2017 trend is estimated at -0.12 ± 0.33 K/dec, although this trend is highly influenced by the strong positive values of the first part of the timeseries.

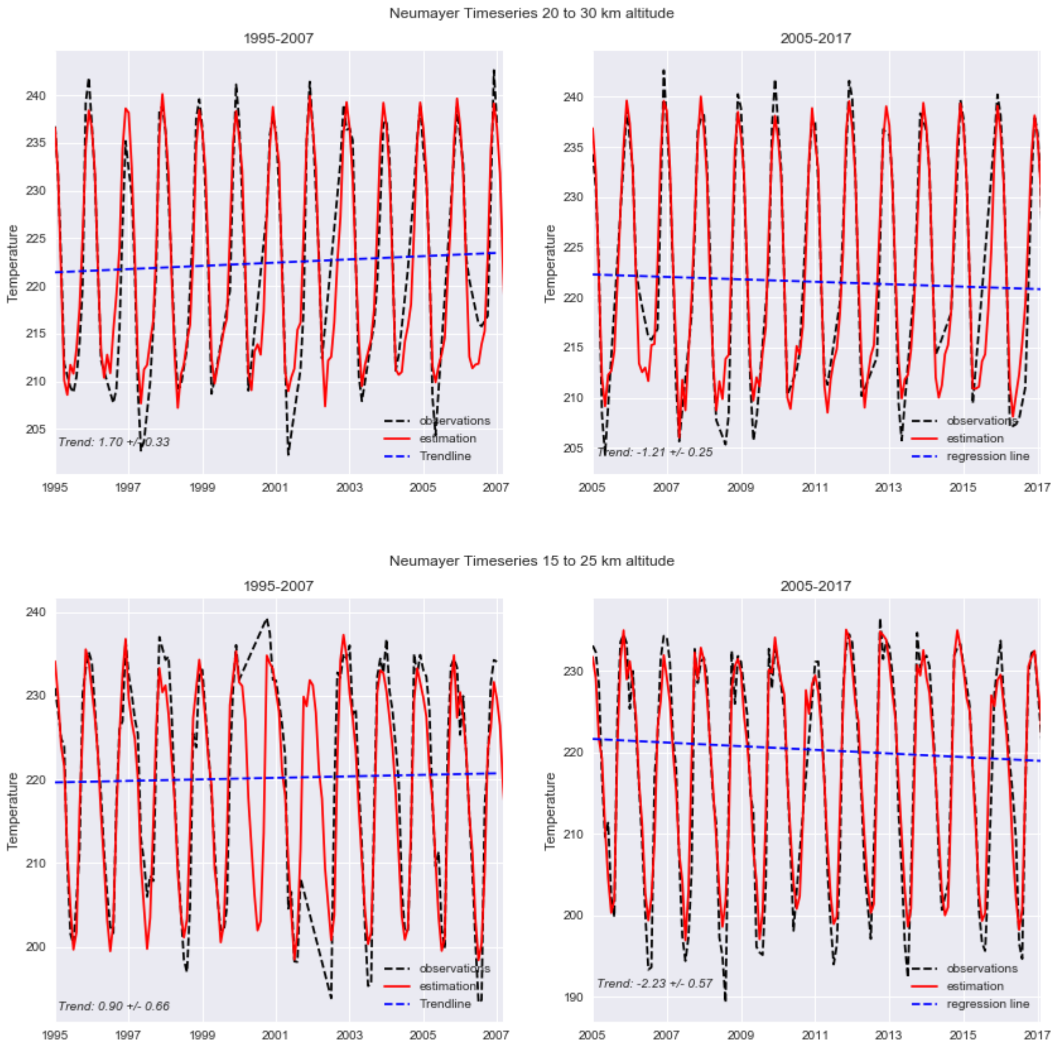

Figure 4.10: *Same as figure 4.9 but for Neumayer station.*

The ozone contribution is comparable to Dumont, which is to be expected since the same ozone profile is used as input. O_3 trends are $+0.26 \pm 0.09$ K/dec and $+0.48 \pm 0.19$ K/dec for both altitude bins in the Neumayer station.

The eigenvectors, shown in table 4.10, have very similar projections and magnitudes as the Dumont eigenvectors. The modes for each eigenvector are thus explained in the same fashion, CO_2 is the leading mode in determining the temperature trend in the timeseries.

Table 4.10: *SVD eigenvectors (λ) of the Neumayer timeseries, showing the correlation of different processes on Temperature, O_3, CO_2 and the incoming Solar flux. Eigenvectors for the period 1995-2017.*

	λ_1	λ_2	λ_3	λ_4
Temperature	-0.61	-0.43	0.24	0.61
Ozone	0.25	0.32	0.90	0.12
CO2	0.68	-0.14	-0.23	0.67
Solar	-0.30	0.82	-0.26	0.38
Eig.value	0.67	0.20	0.11	0.02

Boulder

The Boulder reconstructed timeseries are portrayed in figure 4.11. Trends for both altitude bins are weakly negative. Overall, the 20-30 km altitude bin shows cooling: -0.09 $\pm$ 0.4 K/dec. The trend model detects very small and uncertain trends for the lower stratosphere. Likewise the Lauder timeseries in the lower stratosphere, the Boulder observations show large variability in the lowest altitude bin. The temperature pattern is much more irregular than at higher altitudes. Tropospheric influence is clearly present here. The antarctic observations do not show this type of variability in this altitude bin. This can be explained by a more stable Antarctic stratosphere, by the lower location of the tropopause at higher latitudes and due to the nearby Rocky Mountains, which form a topographic barrier where instabilities are triggered that can travel upward.

The ozone column above Boulder is comparable with the Lauder profile, although the net increase for boulder is higher, approximately 0.8%/dec. Despite this net increase, the trend model does not appoint a significant trend to this ozone increase. The net ozone induced trend, according to the trend model is effectively zero.

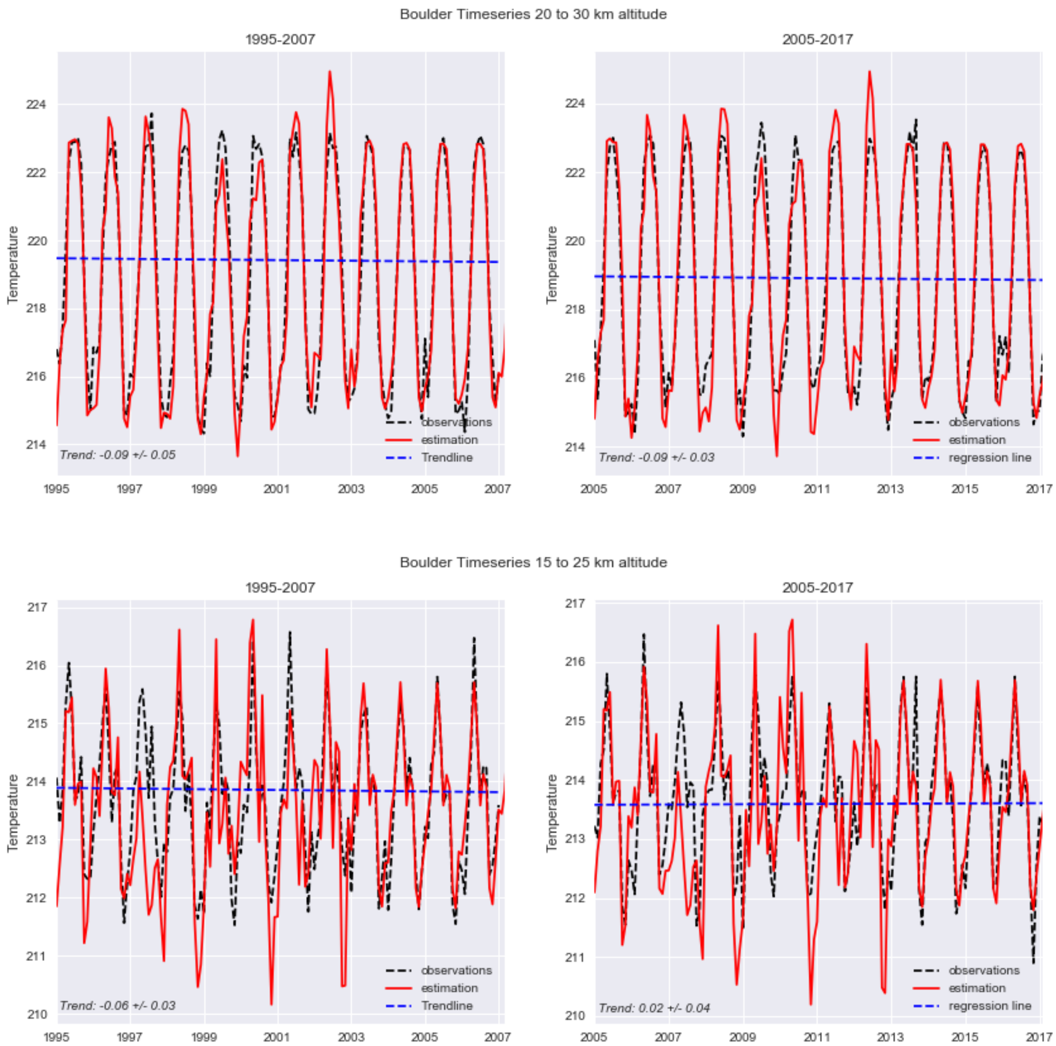

Figure 4.11: *Reconstructed timeseries for Boulder, upper panels show 20-30 km, lower panels show 15-25 km altitude bin.*

The first eigenvector has an eigenvalue of 0.49. This eigenvector has a strong projection on temperature and involves an anti correlation between temperature and the other variables. A underlying process for this mode of variability is not obvious since no process correlates equally on CO_2 and O_3 but negatively on temperature. The variability due to tropospheric influence is thus appointed as the cause for this mode of variation. The second eigenvector has a strong projection on CO_2 and the solar flux. Despite the relatively weak projection on temperature, this mode is associated with the CO_2 concentration. The negative correlation with the solar cycle can be explained by the fact that the second amplitude of the cycle is much lower than the first. The weak ozone correlation is explained by the negative feedback of slowing ozone destruction, as explained. The third mode of variation is interpreted as changes in ozone column. Directions on temperature and O_3 are equal. The SVD shows that for the Boulder timeseries, the greenhouse gas component is not as dominant as in the Antarctic timeseries. Additionally, the observations include a mode of unknown variability, interpreted as tropospheric influences and a small contribution of ozone.

Table 4.11: *SVD eigenvectors (λ) of the Boulder timeseries, showing the correlation of different processes on Temperature, O_3, CO_2 and the incoming Solar flux. Eigenvectors for the period 1995-2017.*

	λ_1	λ_2	λ_3	λ_4
Temperature	0.73	-0.15	0.26	-0.60
Ozone	-0.57	-0.09	0.73	-0.34
CO2	-0.31	-0.62	-0.54	-0.45
Solar	-0.18	0.75	-0.30	-0.54
Eig.value	0.49	0.40	0.10	0.01

Greenland

The Greenland observations are characterised by several strong outliers which are especially large in amplitude in the lower part of the profiles where the seasonal amplitude is doubling throughout the timeseries. These outliers dominate the lower profile and the 30-40 km altitude bin. Therefore, for this timeseries only a 35-50 kilometre profile was taken. Additionally, there are extensive periods without measurements. This means the Greenland observations have to interpreted with caution. The figure **??** shows the reconstructed timeseries. The timeseries contains two negative temperature trends of -1.85 $\pm$ 0.18 and 0.23 $\pm$ 0.53 K/dec. Outliers to low temperatures are still present in the timeseries. The temperature trends are comparable to the trends found in Lauder for the time period 1995-2007 in the upper Stratosphere.

Greenland faced the largest increase of ozone column of all observation stations: 2.3% over the 1995-2015 time period. However, ozone induces a cooling effect on the first part of the Greenland timeseries, this effect is estimated at -0.42 $\pm$ -0.47 K/dec. For 2005-2015, the ozone induced trend fluctuates around zero with a uncertainty of 0.47 K/dec. The overall ozone trend is estimated at -0.12 $\pm$ 0.2 K/dec. Combined with the solar contributions, the net trend in Greenland is strongly negative from 1995-2007: -2.4 $\pm$ 0.47 K/dec but halts in the second part of the timeseries and becomes practically zero. This is also visible in the observations, where a clear downward trend is visible in the first few years which stagnates later on

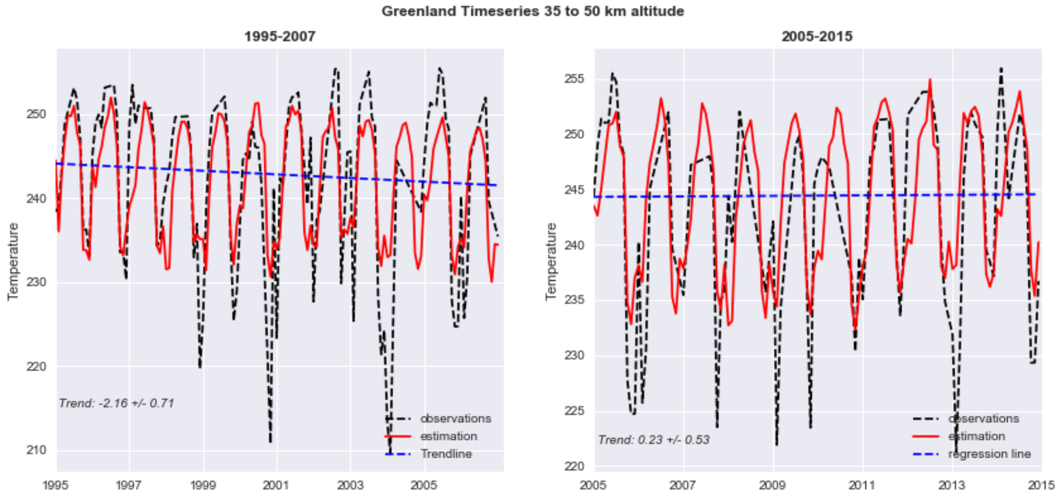

Figure 4.12: *the Greenland reconstructed timeseries for the 35-50 km altitude.*

The eigenvectors show similar values as the upper part of the Lauder series. The first eigenvector has a strong projection on O_3 and temperature. This is thus interpreted to be the ozone imprint on the temperature and ozone variability. Strangely, reversed to the Lauder upper stratosphere, this mode is dominant over the CO_2 mode, which is given by the second eigenvector. For the second mode, CO_2 has an anti-correlation with temperature and is the dominant component of the eigenvector. The corresponding eigenvalue is half as large as the first, indicating that for the Greenland timeseries, the ozone variability should explain more variance in the temperature timeseries than CO_2, however, this is not found by the trend model. The third eigenvalue projects in a comparable magnitude to CO_2, O_3 and the solar flux. A possible mechanism for this mode is the Brewer Dobson circulation, which increases ozone values but does not particularly change carbon dioxide and the solar flux.

Table 4.12: *SVD eigenvectors (λ) of the Greenland timeseries, showing the correlation of different processes on Temperature, O_3, CO_2 and the incoming Solar flux. Eigenvectors for the period 1995-2017.*

	λ_1	λ_2	λ_3	λ_4
Temperature	0.69	-0.10	0.14	0.69
Ozone	-0.64	0.10	0.51	0.55
CO2	-0.07	0.74	-0.58	0.31
Solar	-0.31	-0.64	-0.60	0.33
Eig.value	0.63	0.30	0.06	0.01

Overview

Five different datasets have been analysed. Boxplots 4.13 and 4.14 summarize the detected trends of the observational dataseries.

1. Compared with other observations, the Lauder dataset seems to fall somewhat in between the Boulder and Antarctic datasets for the lower two altitude bins (See figures 4.13 and 4.14 left panels.

2. For the upper altitude bins, the Lauder timeseries only agree with the Greenland timeseries for the 1995-2007 time period. After this the Lauder timeseries become positive which is not the case in the Greenland observations. See right panels of figures 4.13 and 4.14.

3. The Antarctic stations contain significant temperature trends, for both altitude bins of 15-25 and 20-30 km. Although the Neumayer station contains a positive trend value from 1995-2007, this is regarded as insignificant due to missing uncertainty in the data. Additionally, from 1995-2017, the Neumayer station also shows negative trend.

4. Ozone trends are weakest in Lauder. The trend model estimates warming associated with ozone the largest for the Antarctic timeseries. Lauder ozone induced trend values fall in between both stations but are closer to Boulder values.

5. The Greenland observations contain trends that are the largest of all observational timeseries. However, these have to be interpreted with caution due to large fluctuations in observational data. The 35-50 km altitude shows strong negative trends induced by greenhouse gas trends.

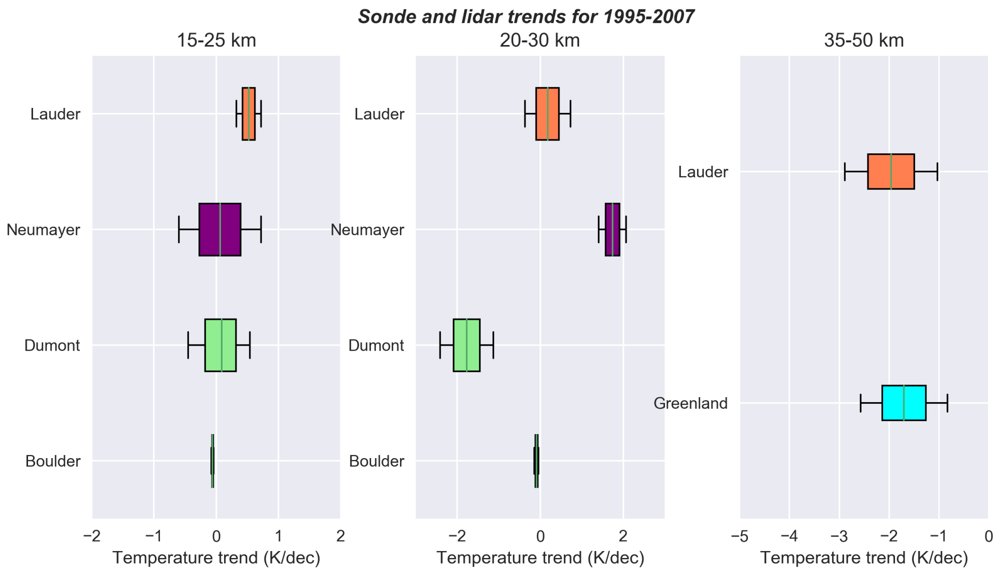

Figure 4.13: *Boxplot portraying the trends found at the temperaturesets from the Sonde and Lidar profiles. Whiskers give the spread, plus and minus one standard deviation from the mean trend.*

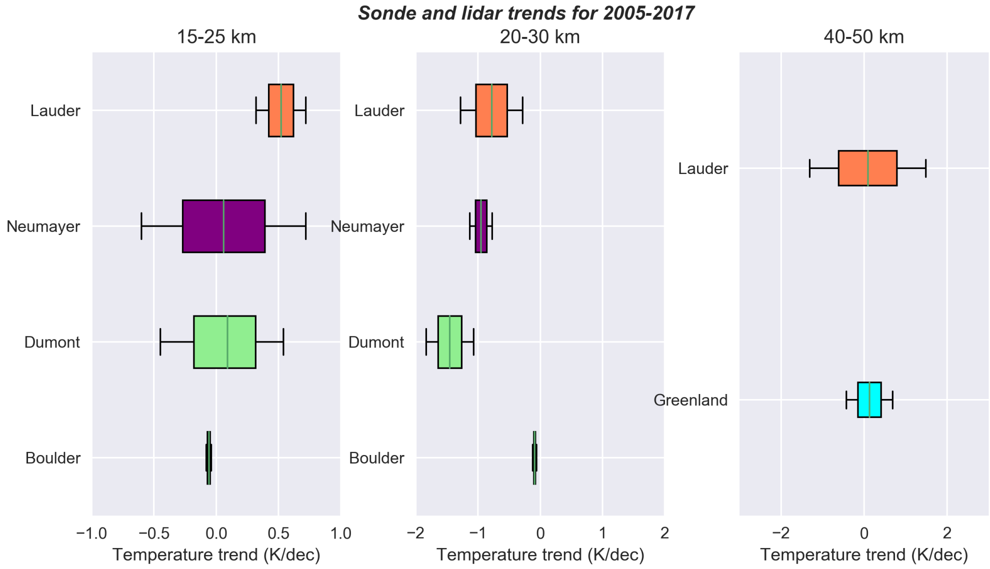

Figure 4.14: *Same as 4.13, but for the time period 2005-2017. The Greenland Lidar timeseries only continue until 2015.*

The Singular Value Decomposition showed that overall, CO_2 is the leading component determining the trends in the temperature series. The role of CO_2 in the temperature trends is estimated to be a 3-4 times larger than the O_3 component. This is mainly based on the Antarctic datasets and the upper stratosphere in the Lauder observations.

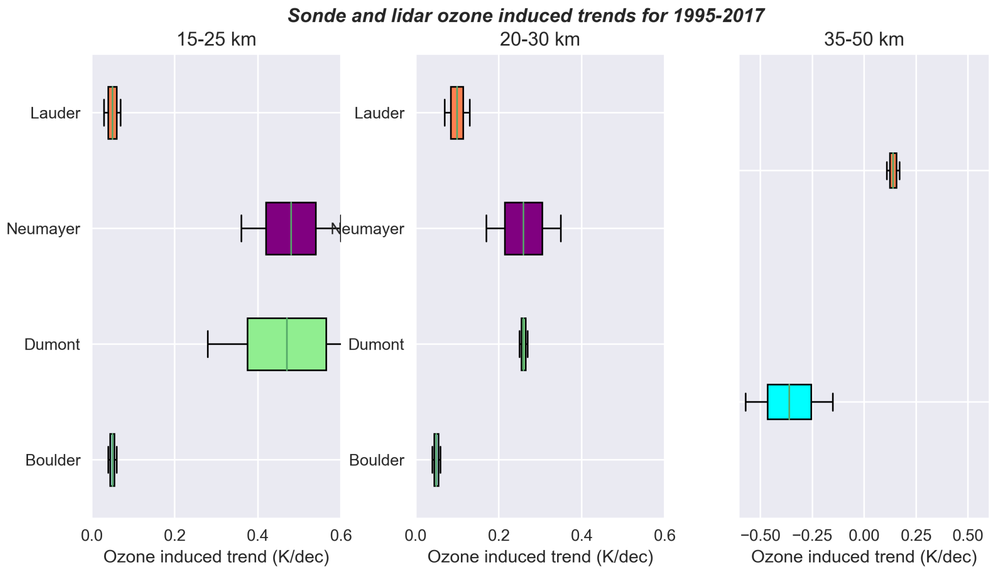

Figure 4.15: *Ozone induced trends as found by the trend model for the different observations.*

4.3 CMIP models

If we want to find a projection of future changes in Stratospheric temperatures, the CMIP models of the IPCC can be used. The CMIP5 consists of General Circulation Models which are compared to give estimations of changes in global climate due to anthropogenic forcings. The CMIP5 models contain less noise and short term variability as the measuremened profiles and do not suffer from calibration or experimental errors. The CMIP5 data can therefore be regarded as an idealised dataset. Comparing CMIP5 output with the observations and consecutively running the trend model on the CMIP5 output might give additional information stratospheric temperature trend. The CMIP5 models can be compared with the Lauder values to gain more insight in the trend model output. The CMIP5 models picked to be compared with the Lauder dataset must have accurate descriptions of ozone levels and have sufficient vertical resolution in the stratosphere. All but one of the CMIP5 models have an interactive ozone chemistry model. Interactive ozone chemistry means that ozone is calculated online for every timestep. The NASA-GISS model, which does not have interactive ozone chemistry uses prescribed ozone values, the database for the ozone values is available at [Schmidt et al., 2006].

Figure 4.16 shows the comparison of the CMIP5 data with the Lauder Lidar data. The data are plotted for different heights within the MSU and SSU altitude bins. The CMIP5 model output consist of historical runs until 2005, after this the modelled data follow the RCP 4.5 pathway. The timeseries in figure 4.16 show that models underestimate the Upper Stratospheric temperatures. Especially during summer and around the 7 hPa pressure level (40 kilometres), models perform poor, underestimating temperatures up to 20 Kelvin. The underestimation of temperature is present throughout the timeseries. For the middle and lower stratosphere, CMIP5 models more accurately resemble the observations, with smaller temperature underestimations. At these levels, intraseasonal fluctuations become more dominant. This is also visible in the CMIP5 data. The sum of residuals per year between the model data and Lauder dataset is larger for the second part of the timeseries. This could either be related to the positive trend in the Lauder temperatures or by a cooling projected by the CMIP5 models. The NASA-GISS model, with prescribed ozone values, does not perform well for altitudes around the ozonelayer (50 hPa).

Although the CMIP5 models do not perform well at the 7 hPa altitude level, the temperatures at other altitudes are captured reasonably well. Moreover, the seasonal temperature tendency and internal variation seems to be simulated fairly accurate. Therefore the models are expected to capture the response of stratospheric temperatures to changes in drivers.

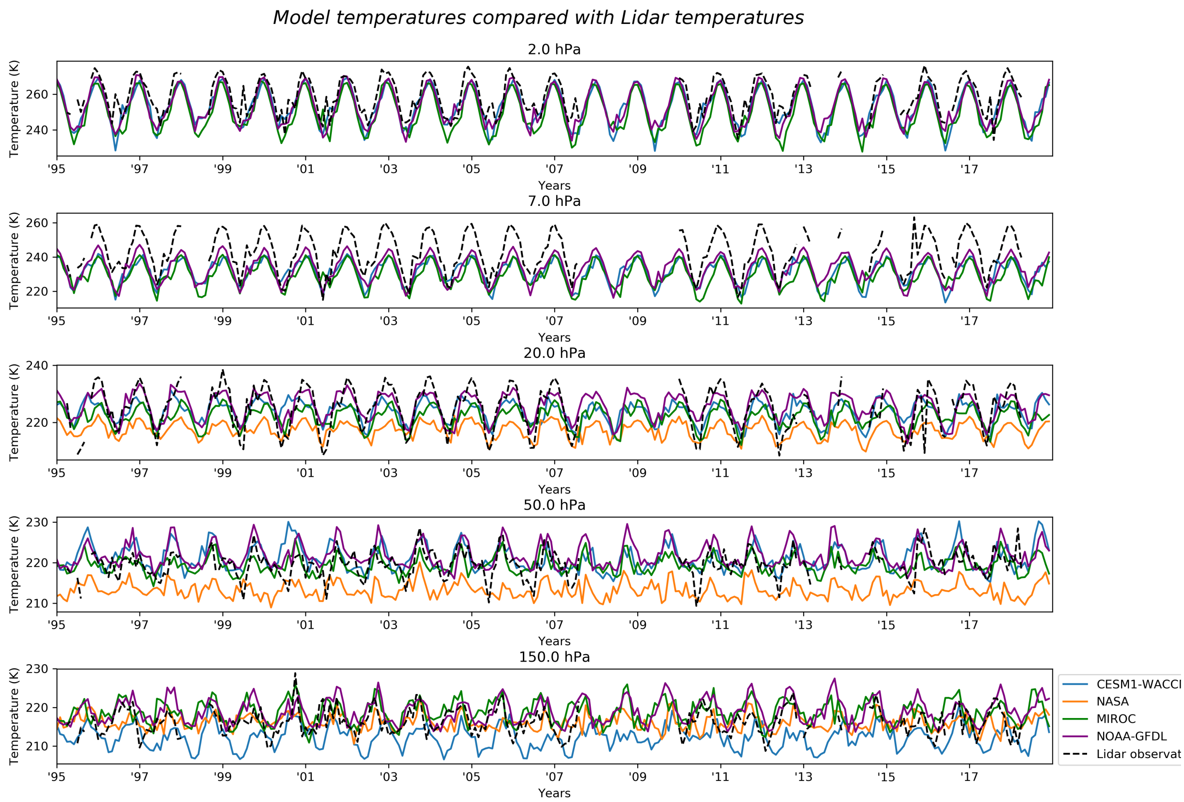

Figure 4.16: *The CMIP5 model data compared with the Lidar observations for different altitudes. The CMIP5 data are taken for the gridcells surrounding and overlapping with the location of Lauder. From top to bottom: 2 hPa: 49 kilometres, 7 hPa: 40 kilometres, 20 hPa: 31 kilometres, 50 hpA: 24 kilometres and 150 hPa: 15 kilometres altitude. The CMIP5 data are based on observed emissions and parameters untill 2005 (historical runs). From 2006, the CMIP data follow the RCP 4.5 scenario. The Squared Residuals between model data and Lauder data are larger in the second part of the dataset (2005-2017) than in the first dataset. This is caused by an expected cooling trend in the RCP 4.5 scenario due to increased GHG combined with the positive trend in the second part of the timeseries as was found by the trend model.*

To get a quantification of the temperature changes occuring in the different CMIP5 models, the temperature trend model is applied on the CMIP5 datasets. As ozone column input, the model ozone concentrations are recalculated to DU values to represent the ozone component. The QBO proxy values are taken from the modelled zonal winds at equatorial latitudes. The solar component proxy used for the CMIP5 comparison is the 10.7 cm radioflux, equal to the proxy used for trend estimation of the observational timeseries. The trends calculated thus are interpreted to be of greenhouse gas origin.

The output of the trend model for the 'historical' period of 1995-2005 is shown in table 4.13 and for the RCP 4.5 scenario for the period 2006-2018 in table 4.14. Trends are tested for the different altitude bins. All models show negative trends throughout the complete stratosphere. Generally, strongest trends are found in the upper parts of the stratosphere, close to the stratopause. However, several strong negative temperature trends also exists around the ozone layer level. Strongest trends are found in the upper parts of the stratosphere, above 31 kilometres. Of the models extending to the stratopause, the CESM-WACCM model is the only one with a highly uncertain trend at the top of the stratosphere.

Table 4.13: *Trend model performed on the CMIP models for the historical period (1995-2005). Values are given in Kelvin per decade. Uncertainty ranges are +/- one standard deviation. Trend model run includes solar, ozone and qbo changes, trendvalues are thus interpreted as greenhouse gas induced. CESM-FASTCHEM model does not include stratospheric layers above 33 kilometres.*

	Models - Historical			
Altitude	**MIROC-CHEM**	**NOAA-GFDL**	**CESM-WACCM**	**CESM-Fastchem**
15 Km	-0.75 ±0.38	-0.23 ±0.34	-0.25 ±0.38	-0.54 ±0.43
24 Km	-0.53 ±0.25	-0.41 ±0.26	-0.78 ±0.38	-0.5 ±0.38
31 Km	-0.35 ±0.42	-.1.1 ±0.4	-0.7 ±0.49	-0.73 ±.54
42 Km	-0.45 ±0.66	-0.94 ±0.51	-0.7 ±0.3	-
49 Km	-0.9 ±0.64	-0.66 ±0.6	-.01 ±0.77	-

Figure 4.14 shows the found temperature trends for RCP 4.5 scenario. The RCP 4.5 scenario predicts a CO_2 abundance of 411 ppm by 2020. The RCP 4.5 scenario trends are, on average, smaller than the trends that that were found in the historical period. This is is due to the effect of ozone recovery, which is projected to occur from the early 00's in all RCP scenarios'. Despite the ozone recovery the trends are still significantly negative throughout the stratosphere. Model thus point to the stronger effect of CO_2 than due to recovering ozone. The rates of cooling are several orders larger than tropospheric temperature change which is on the order of 0.1-0.2 K/dec.

Table 4.14: *Trend model performed on the CMIP5 models for the RCP 4.5 trends. Values are given in Kelvin per decade and are using ozone values as input in order to keep only the Greenhouse gas signature in the trend. CESM-FASTCHEM model does not include stratospheric layers above 33 kilometres*

	Models - RCP 4.5			
Altitude	**MIROC-CHEM**	**NOAA-GFDL**	**CESM-WACCM**	**CESM-FASTCHEM**
15 Km	-0.78 ±0.34	-0.10 ±0.12	-0.10 ±0.11	-0.18 ± -0.11
24 Km	-0.51 ±0.21	-0.51 ±0.19	-0.58 ±0.21	-0.55 ± -0.17
31 Km	-0.41 ±.38	-0.80 ±0.47	-0.80 ±0.33	-0.71 ± -0.35
42 Km	-0.23 ±0.54	-0.84 ±0.46	-0.56 ± -0.40	-
49 Km	-0.18 ± -0.48	-0.95 ±0.52	-0.13 ± -0.35	-

As is visible in tables 4.13 and 4.14, the CMIP models show trends that support theoretical studies and assumptions [Andrews et al., 1987],[Fels et al., 1980]. The cooling, induced by greenhouse gasses is clear and fairly uniform in all models. Compared with literature, the trends of the historical CMIP5 series are within the uncertainty range of the trends found by [Maycock et al., 2018],[Maycock, 2016b],[Mitchell, 2016], based on AMSU and SSU data. The MIROC and GFDL models are on the higher end of trends reported by by these papers. AMSU and SSU data mean trend values are between -0.5

and - 1.0 K/dec, which are trends not filtered for ozone values.

The model means of the historical runs and the different projected scenarios are shown in the boxplot (figure 4.17). Clearly visible is that the CMIP5 models contain far less uncertainty for all time periods. Also visible is that the CMIP5 models, and RCP 4.5 and 8.5 scenario's show a temperature trend distribution in which the trend is stable or slightly increases with height. In the historical period, portrayed in the left panel of figure 4.17, the Lauder trends are on the extreme sides of the model mean trends. Stronger and negative for the upper stratosphere and positive in the lower stratosphere. For the 2005-2017 period, the Lauder dataset shows the most similarity with the RCP 6.0 scenario, in this scenario, temperature trends in the stratosphere are positive, especially higher in the atmosphere.

projections/Boxplotearly.png projections/Boxplot2005-2017.png

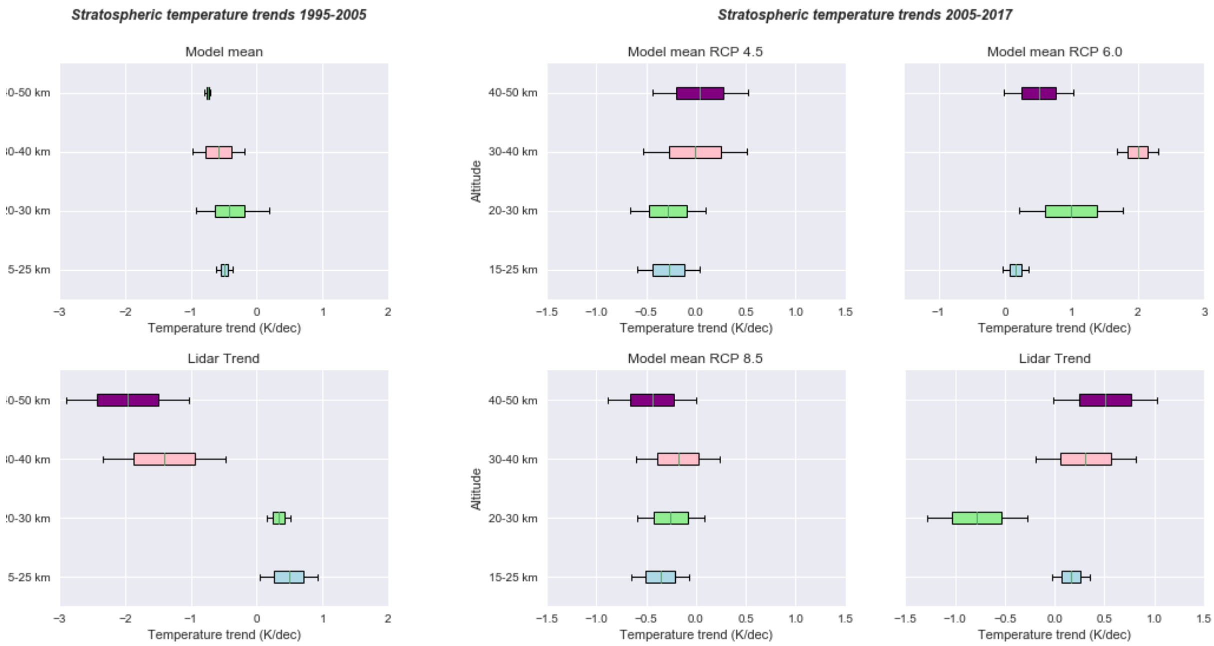

Figure 4.17: *Trends of the different model output, compared to the Lidar output, averaged over altitudes corresponding to the different altitude bins. Left panels shows the historical runs of the CMIP5 models. The right panels show the different scenario's from 2006-2017 compared to the Lauder trend values.*

Since abundance of the dominant greenhouse gasses and changes in the ozone column does not differ very much within the different scenario's before 2020, it is also interesting to plot the stratospheric temperatures for longer time periods, where changes do become clear. Figure 4.18 shows stratospheric temperatures until 2050 under the different scenario's. Temperatures are normalised for the observed temperatures according to the Lauder temperature set and connected to the observational means for the 1995-2005 period. Changes in stratospheric temperatures stay limited within -1 Kelvin for the RCP 4.5 scenario and run up to - 3K for the RCP 8.5 scenario. Compared to the 1975-2005 mean, as is done in the IPCC reports, anomalies are approximately -2.5 and -5.5 K.

projections/RCPscenarios2hPa.png

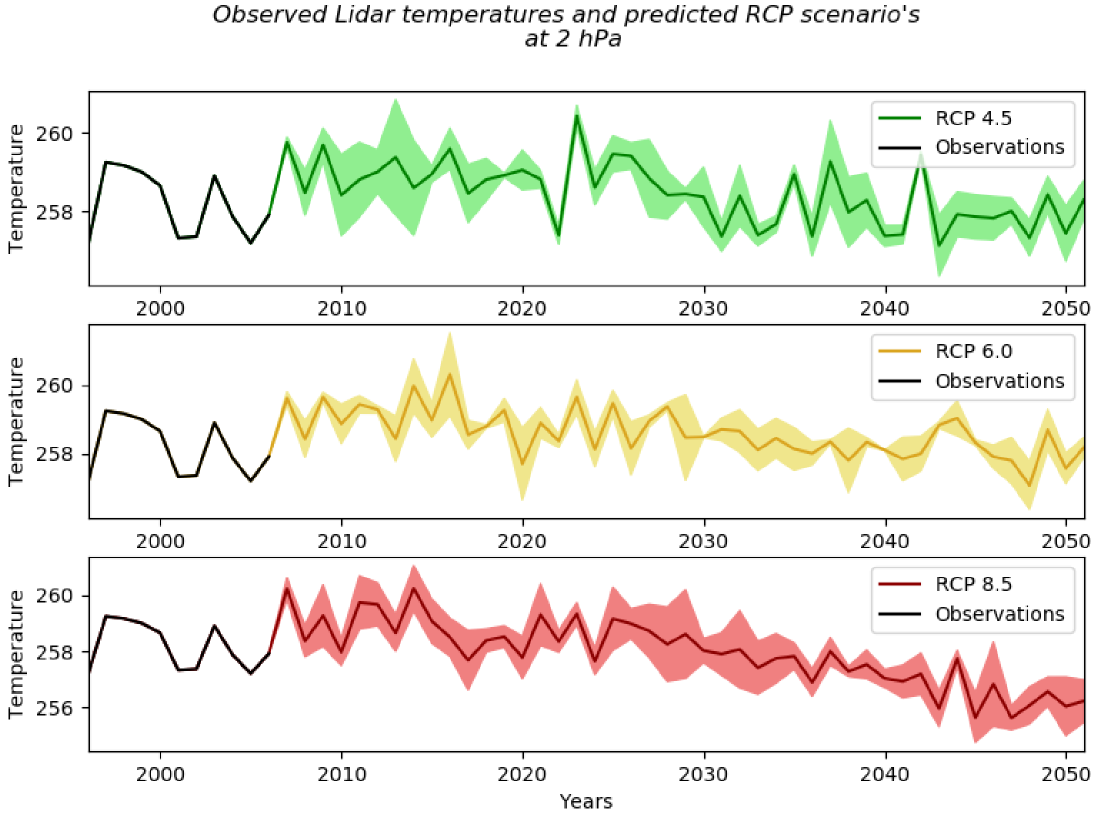

Figure 4.18: *Yearly mean temperatures, from the 1995-2005 mean. Temperatures are corrected for differences in model and lidar values.*

5 Conclusion and discussion

The Lauder temperature profiles, that were derived by an RIVM Lidar between 1995 and 2017, were compared with other retrieved temperature observations from different measurement stations and compared with CMIP5 model data. It was discovered that significant temperature trends exist in the Lauder observations, the magnitude of which differs throughout the stratosphere. To get back to the research questions stated, the conclusions regarding the different trends and the comparison with CMIP5 models and other observations are described per altitude range.

15-25 km

In the lower stratosphere, the Lauder temperature timeseries holds positive temperature trends. For 1995-2007 and 2005-2017, temperature trends of 0.53 ± 0.22 and 0.41 ± 0.13 K/dec were found. The magnitude of positive trends in the Lauder series is unique for this altitude range. Boulder, which is latitudinally the most related to Lauder, but located in the Northern Hemisphere, contains a insignificant trend of approximately -0.05 ± 0.4 K/dec. Both timeseries show strong short scale variability, caused by tropospheric influences. Upward travelling tropospheric disturbances are also thought to be of influence in the Lauder timeseries. The variability in the timeseries is reflected in the first and second modes of variance derived with an SVD method. For Boulder and Lauder these two modes project strongly on temperature and show an anti correlation between both ozone and CO_2. The Antarctic stations are dominated by negative temperature trends which vary in magnitude from several tenths of degrees to almost 2.0 K/dec. For both Antarctic stations, the timeseries contain much less inter annual variability due to the lower altitude of the tropopause.

The trends detected in the CMIP5 models have a much smaller uncertainty range than the observations. The CMIP5 average trend is approximately -0.6 K/dec until 2005 and -0.4 K/dec for 2005-2017. Compared with observations, the CMIP5 imposed greenhouse gas trend seems somewhat large. However, CMIP5 models are comparable to satellite instrument reconstructions [Maycock et al., 2018][Seidel et al., 2011][Maycock, 2016b][Mitchell, 2016] and small compared to the Antarctic temperature trends. Therefore it can be concluded that either the temperature trends found in the Lauder lower stratosphere are not representative for the global lower stratosphere temperature changes. The presence of inter annual variability might obscure the actual CO_2 trend existing. This makes the trend detected by the trend model not plausible to be of CO_2 origin. Tropospheric disturbances and additional stratospheric dynamics are necessary to account for the positive trend.

20-30 km

The middle stratosphere I altitude bin of the Lauder timeseries contains a positive, uncertain trend of 0.18 ± 0.22 K/dec from 1995-2007 and a larger, significant trend of -0.86 ± 0.07. This gives a average trend of -0.57 ± 0.26 for the 1995-2017 time period. The 1995-2017 trend is similar values found by Maycock et al, (2018), Aquila et al, (2016) and Mitchell (2016) for the CO_2 induced cooling . The Boulder timeseries contains weaker trends. Estimated trendvalues are -0.1 ± 0.04 K/dec for the 1995-2017 time period. Both Antarctic timeseries contain strong negative trends for this part of the stratosphere. If the single positive Neumayer trend is neglected, for which plausible reasons were given in section 4.1.3, the Antarctic trends are estimated at -1.0 to -1.8 ± 0.6 K/dec. Compared with other observations, the Lauder trend values are in between the boulder and Antarctic values.

CMIP5 historical runs (1995-2005), contain trends of -0.5 ± 0.3 K/dec. For the RCP 4.5 and 8.5 scenario's, this magnitude persists and thus matches very well with the Lauder estimation. The RCP 6.0 scenario is the only timeseries that projects increasing stratospheric temperatures. Looking at the relatively good agreement between the Lauder observations with satellite research and CMIP5 model output, it can be concluded that the stratosphere is cooling in the 20-30 km altitude range and that the Lauder timeseries is representative for cooling rates at corresponding latitudes. The Antarctic trends are found to be much larger, for these stations, additional factors might be of influence on the detected trend, although Maycock et al., (2018) mention a stronger cooling signal at Antarctica compared to global means.

30-40 km

Lauder observations contain a trend of -0.40 ± 0.33 K/dec between 1995-2007 and 0.04 ± 0.15 for 2005-2017. This leads to a complete timeseries trend of -0.18 ± 0.15 K/dec. This temperature trend is on the low side of estimations by Aquila et al., (2016) and Mitchell et al, (2016) on the CO_2 cooling component. Since no adequate observations were found, this altitude bin lacks comparison with other observational datasets. The SVD analysis led to the conclusion that solar variability has a significant influence on the temperature variance. However, this statement has to be taken with caution since only two solar cycles are included in the timeseries, the second of which is much smaller in amplitude than the first.

CMIP5 cooling rates for the 1995-2005 time period average -0.7 ± 0.3 K/dec. Predicted trends for 2006-2017 are more conservative: -0.4 ± 0.1 K/dec for RCP 4.5 and -0.5 ± 0.15 K/dec for the RCP 8.5. RCP 6.0 again has a warming component. The CMIP5 model cooling rates are overall thus stronger than the lauder temperature trends. The 1995-2007 time period seems to be more accurate in comparison with models and satellite measurements. The second part of the timeseries is regarded as invaluable in detecting a trend in comparison with previous observations. Understanding the dependence of temperatures on implemented instrumental changes are necessary.

40-50 km

Theoretically, the upper stratosphere is expected to contain the strongest temperature trends. This is true from 1995-2007, for which the lauder trend is estimated at -1.46 ± 0.53 K/dec. However, the years 2005-2017 contain positive trends of 0.37 ± 0.16 K/dec which brings the net trend for the complete time period at effectively zero. The Lauder timeseries are only comparable with observations taken from the Greenland Lidar measurements. This temperature record contains continuous greenhouse gas induced trend values of -2.16 ± 0.71 to 0.23 ± 0.53 K/dec. Although the Greenland observations need also to be interpreted with care, despite the removal of the lower part of the profile, large temperature outliers between 2003-2008 still dominate the observations.

Temperature trends in the CMIP5 data for the upper stratosphere are very comparable to those at 30-40 km altitudes. For the 1995-2007 period, trends are somewhat larger, approximately -0.8 K/dec. For the predictions 2006-2017, the magnitude differs between RCP 4.5 and RCP 8.5 from -0.4 to -0.6 K/dec. RCP 6.0 contains a positive trend of 0.4 K/dec, again resembling the Lauder trend for the years 2005-2017 accurately. Similar as with the 30-40 km altitude range, the second time period of the Lauder temperature series seems obscured by lack of observations and adjustments in the Lidar.

Fingerprinting signals

A second aim of the research was to test whether the trend model would be able to detect the ozone and carbon dioxide forcing separately. For all stations it was found that ozone column values increase compared to the 1995 values. The induced ozone warming is predominantly present in the second part of the timeseries ranging from +0.1 K/dec for the Lauder timeseries to +0.6 K/dec in the Dumont observations. Overall, the trend values assigned are plausible and fall within the ranges given by Aquila et al, (2016) and the modelled values by Eyring et al, (2013). However, some of the observed values show discrepancy between one another.

a) The ozone induced temperature trend of Lauder was estimated at 0.1 ± 0.05 K/dec for 1995-2017. For the same period, the Boulder observations do not seem to inhibit an ozone induced trend, despite the larger, relative increase in ozone column above Boulder.

b) The contribution of the change in Greenland ozone column to the temperature trend is estimated at -0.12 ± 0.2 K/dec, which is in conflict with the large increase in ozone column over 2% per decade.

These discrepancies might be due to observational errors or due to flaws in the ability of the trend model to capture separate trends. Since the physical processes behind the temperature increase are not covered by the model, a trend assigned to ozone, could actually be a combination of the CO_2 and ozone effect. Both trends are assumed to be close to linear and can be incorporated by the model into a trend that is assigned to only one of the two drivers. This was tried to be avoided by using ozone column values as input. However, this seems not to be sufficient at all times. Especially with relatively small changes as is the case in Lauder, or with large variability and uncertainty in the temperature values, as is the case in Greenland. Additionally, other dynamics and variables might be important in the Stratosphere. [Randel et al., 2006] mention the influence of changes in water vapor on tropical stratospheric temperatures, which is estimated to contribute to a 1 K/dec warming. Furthermore, [Butchart, 2014] estimate increases in the Brewer Dobson circulation due to anthropogenic greenhouse gas emissions up to 3%/dec. This means transport of ozone, carbon dioxide and water vapor to higher latitudes is increased, however, the resulting influence on temperatures are not explicitly named. Butchart (2014), also names the Quasi Biennial Oscillation as an important factor in the transport of the QBO. Since the trend model does not capture the BDC, water vapor or aerosol changes directly, the trends that have been detected using the trend model must therefore be interpreted as a crude estimation of the CO_2 induced trend.

The Singular Value Decomposition was used as an additional tool to specify the relative importance of different components to the temperature timeseries. However this does not determine the absolute trend values. The SVD did lead to the conclusion that CO_2 is the dominant factor in determining the temperature trend over ozone, this is true for the complete stratosphere. The only exception was found in the Greenland observations in which ozone is interpreted to be the first mode of variability.

Overall, the trend model proved useful for detecting changes in the stratosphere. With a relatively simple approach, different trendcomponents in the observational series can be detected. The advantage of such a trend model is that no general circulation models are necessary to simulate different drivers. Furthermore, no bias in model outcomes have to be accounted for and signals are directly derived from observations. On the contrary, the use of such a trend model makes the results very sensitive to the quality of observations. Accurate trend detection in Lauder turned out to be difficult due to occasionally sparse temporal sampling and uncertainties involved in instrument changes along the observational period. Also, Lidar observations are restricted to night time, clear sky conditions. The bias of these measurement restrictions on the trend estimation is not known. Difficulties involved in the NDACC data that were used to compare to the Lauder timeseries are similar. The NDACC data sometimes lack temporal coverage and are not always documented in a structured way. A second akin study would therefore be recommended to use multiple, well documented measurement series and calibrate the model against proven timeseries to reduce uncertainties. Also additional restraints to guard the separation of different variables could be made to give more clarity on the magnitude of the resulting trend. This could be done by including supplemental parameters could to the trend model, in example aerosol and H_2O values and possibly eddy fluxes to get a better estimation of the Quasi Biennial Oscillation.

Acknowledgements

At first place I would like to thank Guus Velders, who supervised and helped me during this project. Also I would like to thank Anne van Gijsel, and the RIVM for supplying me with the Lidar data that were necessary to do the project. Finally a thank you to my fellow students, with whom it has been great to study with.

Bibliography

[Ajavon et al., 2018] Ajavon, A.-L., Newman, P. A., Pyle, J. A., and Ravishankara, A. R. (2018). Scientific assessment of ozone depletion: 2010. Technical Report 52.

[Andrews et al., 1987] Andrews, D. G., Holton, J. R., and Leovy, C. B. (1987). *Middle Atmosphere Dynamics*. Acadamic Press, Inc., London.

[Angell, 1993] Angell, J. (1993). Comparison of stratospheric warming following agung, el chichon and pinatubo volcanic eruptions. *Geophysical research letters*, 20(8):715–718.

[Angell, 1997] Angell, J. (1997). Stratospheric warming due to agung, el chichón, and pinatubo taking into account the quasi-biennial oscillation. *Journal of Geophysical Research: Atmospheres*, 102(D8):9479–9485.

[Behrendt, 2005] Behrendt, A. (2005). Temperature measurements with lidar. In *Lidar*, pages 273–305. Springer.

[Bjornsson. and Venegas., 1997] Bjornsson., H. and Venegas., S. A. (1997). *A Manual for EOF and SVD Analyses of Climatic Data*, volume XXXIII.

[Butchart, 2014] Butchart, N. (2014). The brewer-dobson circulation. *Reviews of geophysics*, 52(2):157–184.

[de Winter-Sorkina, 1995] de Winter-Sorkina, R. (1995). RIVM report on ozone trends.pdf. Technical report.

[Donner et al., 2011] Donner, L. J., Wyman, B. L., Hemler, R. S., Horowitz, L. W., Ming, Y., Zhao, M., Golaz, J.-C., Ginoux, P., Lin, S.-J., Schwarzkopf, M. D., et al. (2011). The dynamical core, physical parameterizations, and basic simulation characteristics of the atmospheric component am3 of the gfdl global coupled model cm3. *Journal of Climate*, 24(13):3484–3519.

[Eyring et al., 2013] Eyring, V., Arblaster, J. M., Cionni, I., Sedláček, J., Perlwitz, J., Young, P. J., Bekki, S., Bergmann, D., Cameron-Smith, P., Collins, W. J., Faluvegi, G., Gottschaldt, K. D., Horowitz, L. W., Kinnison, D. E., Lamarque, J. F., Marsh, D. R., Saint-Martin, D., Shindell, D. T., Sudo, K., Szopa, S., and Watanabe, S. (2013). Long-term ozone changes and associated climate impacts in CMIP5 simulations. *Journal of Geophysical Research Atmospheres*, 118(10):5029–5060.

[Farman et al., 1985] Farman, J. C., Gardiner, B. G., and Shanklin, J. D. (1985). Together With a -1.6. *Nature*, 315:207–210.

[Fels et al., 1980] Fels, S., Mahlman, J., and Sinclair, R. (1980). Stratospheric sensitivity to perturbations in o3 and co2: Radiative and dynamical response. *Journal of the Atmospheric Sciences*, 37:2265–2297.

[Ferraro et al., 2015] Ferraro, A. J., Collins, M., and Lambert, F. H. (2015). A hiatus in the stratosphere? *Nature Climate Change*, 5(6):497–498.

[Gent et al., 2011] Gent, P. R., Danabasoglu, G., Donner, L. J., Holland, M. M., Hunke, E. C., Jayne, S. R., Lawrence, D. M., Neale, R. B., Rasch, P. J., Vertenstein, M., et al. (2011). The community climate system model version 4. *Journal of Climate*, 24(19):4973–4991.

[Goessling and Bathiany, 2016] Goessling, H. F. and Bathiany, S. (2016). Why co2 cools the middle atmosphere–a consolidating model perspective. *Earth System Dynamics*, 7(3):697–715.

[Hauchecorne and Chanin, 1980] Hauchecorne, A. and Chanin, M.-L. (1980). Density and Temperature Profiles Obtained by Lidar Between 35 and 70 km. *Geophysical Research Letters*, 7(8):565–568.

[Holton, 2004] Holton, J. (2004). *An Introduction to Dynamic Meteorology*. International Geophysics. Elsevier Science.

[Kidston et al., 2015] Kidston, J., Scaife, A. A., Hardiman, S. C., Mitchell, D. M., Butchart, N., Baldwin, M. P., and Gray, L. J. (2015). Stratospheric influence on tropospheric jet streams, storm tracks and surface weather. *Nature Geoscience*, 8(6):433–440.

[Lacis and Hansen, 1973] Lacis, A. A. and Hansen, J. E. (1973). A Parameterization for the Absorption of Solar Radiation in the Earth's Atmosphere. *Journal of the Atmospheric Sciences*, 31:118 – 133.

[Leblanc et al., 2016] Leblanc, T., Sica, R. J., Van Gijsel, J. A., Godin-Beekmann, S., Haefele, A., Trickl, T., Payen, G., and Liberti, G. (2016). Proposed standardized definitions for vertical resolution and uncertainty in the ndacc lidar ozone and temperature algorithms–part 2: Ozone dial uncertainty budget.

[Manabe and Wetherald, 1967] Manabe, S. and Wetherald, R. T. (1967). Thermal Equilibrium of the Atmosphere with a Given Distribution of Relative Humidity. *Journal of the Atmospheric Sciences*, 24(3).

[Matthes et al., 2010] Matthes, K., Marsh, D. R., Garcia, R. R., Kinnison, D. E., Sassi, F., and Walters, S. (2010). Role of the qbo in modulating the influence of the 11 year solar cycle on the atmosphere using constant forcings. *Journal of Geophysical Research: Atmospheres*, 115(D18).

[Maycock, 2016a] Maycock, A. C. (2016a). The contribution of ozone to future stratospheric temperature trends. *Geophysical Research Letters*, 43(9):4609–4616.

[Maycock, 2016b] Maycock, A. C. (2016b). The contribution of ozone to future stratospheric temperature trends. *Geophysical Research Letters*, 43(9):4609–4616.

[Maycock et al., 2014] Maycock, A. C., Joshi, M. M., Shine, K. P., Davis, S. M., and Rosenlof, K. H. (2014). The potential impact of changes in lower stratospheric water vapour on stratospheric temperatures over the past 30 years. *Quarterly Journal of the Royal Meteorological Society*, 140(684):2176–2185.

[Maycock et al., 2018] Maycock, A. C., Randel, W. J., Steiner, A. K., and Karpechko, A. Y. (2018). Revisiting the Mystery of Recent Stratospheric Temperature Trends. *Geophysical Research Letters*, pages 9919–9933.

[Maycock et al., 2011] Maycock, A. C., Shine, K. P., and Joshi, M. M. (2011). The temperature response to stratospheric water vapour changes. *Quarterly Journal of the Royal Meteorological Society*, 137(657):1070–1082.

[Mitchell, 2016] Mitchell, D. M. (2016). Attributing the forced components of observed stratospheric temperature variability to external drivers. *Quarterly Journal of the Royal Meteorological Society*, 142(695):1041–1047.

[Randel et al., 2009] Randel, W. J., Shine, K. P., Austin, J., Barnett, J., Claud, C., Gillett, N. P., Keckhut, P., Langematz, U., Lin, R., Long, C., Mears, C., Miller, A., Nash, J., Seidel, D. J., Thompson, D. W., Wu, F., and Yoden, S. (2009). An update of observed stratospheric temperature trends. *Journal of Geophysical Research Atmospheres*, 114(2):1–21.

[Randel et al., 2006] Randel, W. J., Wu, F., Voemel, H., Nedoluha, G. E., and Forster, P. (2006). Decreases in stratospheric water vapor after 2001: Links to changes in the tropical tropopause and the brewer-dobson circulation. *Journal of Geophysical Research: Atmospheres*, 111(D12).

[Ribes et al., 2009] Ribes, A., Azaís, J. M., and Planton, S. (2009). Adaptation of the optimal fingerprint method for climate change detection using a well-conditioned covariance matrix estimate. *Climate Dynamics*, 33(5):707–722.

[Schmidt et al., 2006] Schmidt, G. A., Ruedy, R., Hansen, J. E., Aleinov, I., Bell, N., Bauer, M., Bauer, S., Cairns, B., Canuto, V., Cheng, Y., et al. (2006). Present-day atmospheric simulations using giss modele: Comparison to in situ, satellite, and reanalysis data. *Journal of Climate*, 19(2):153–192.

[Seidel et al., 2011] Seidel, D. J., Gillett, N. P., Lanzante, J. R., Shine, K. P., and Thorne, P. W. (2011). Stratospheric temperature trends: Our evolving understanding. *Wiley Interdisciplinary Reviews: Climate Change*, 2(4):592–616.

[Seinfeld and Pandis, 2016] Seinfeld, J. H. and Pandis, S. N. (2016). *Atmospheric chemistry and physics: from air pollution to climate change*. John Wiley & Sons.

[Shindell et al., 2013] Shindell, D. T., Pechony, O., Faluvegi, G. S., Voulgarakis, A., Nazarenko, L. S., Lamarque, J.-F., Bowman, K., Milly, G. P., Kovari, W., Ruedy, R., et al. (2013). Interactive ozone and methane chemistry in giss-e2 historical and future climate simulations.

[Steinbrecht et al., 2009] Steinbrecht, W., Claude, H., Schönenborn, F., McDermid, I. S., Leblanc, T., Godin-Beekmann, S., Keckhut, P., Hauchecorne, A., Van Gijsel, J. A., Swart, D. P., Bodeker, G. E., Parrish, A., Boyd, I. S., Kämpfer, N., Hocke, K., Stolarski, R. S., Frith, S. M., Thomason, L. W., Remsberg, E. E., Von Savigny, C., Rozanov, A., and Burrows, J. P. (2009). Ozone and temperature trends in the upper stratosphere at five stations of the network for the detection of atmospheric composition change. *International Journal of Remote Sensing*, 30(15-16):3875–3886.

[Swart et al., 2002] Swart, D., Spakman, J., J.B., B., E.J., B., and Ormel, F. (2002). RIVM Stratospheric Ozone LIDAR for NDSC Station Lauder, New Zealand. Technical report.

[Vanderwyk, 1975] Vanderwyk, E. (1975). Fluorocarbons and the environment. report of federal task force on inadvertent modification of the stratosphere.

[Varotsos, 2004] Varotsos, C. (2004). The extraordinary events of the major, sudden stratospheric warming, the diminutive antarctic ozone hole, and its split in 2002. *Environmental Science and Pollution Research*, 11(6):405.

[Visser and Molenaar, 1995] Visser, H. and Molenaar, J. (1995). Trend estimation and regression analysis in climatological time series: an application of structural time series models and the Kalman filter.

[Watanabe et al., 2011] Watanabe, S., Hajima, T., Sudo, K., Nagashima, T., Takemura, T., Okajima, H., Nozawa, T., Kawase, H., Abe, M., Yokohata, T., et al. (2011). Miroc-esm: model description and basic results of cmip5-20c3m experiments. *Geoscientific Model Development Discussions*, 4(2):1063–1128.

[WMO, 1988] WMO, W. M. O. (1988). Report of the International Ozone Trends Panel: 1988 (Volume 1). Technical report.

5.1 Appendix

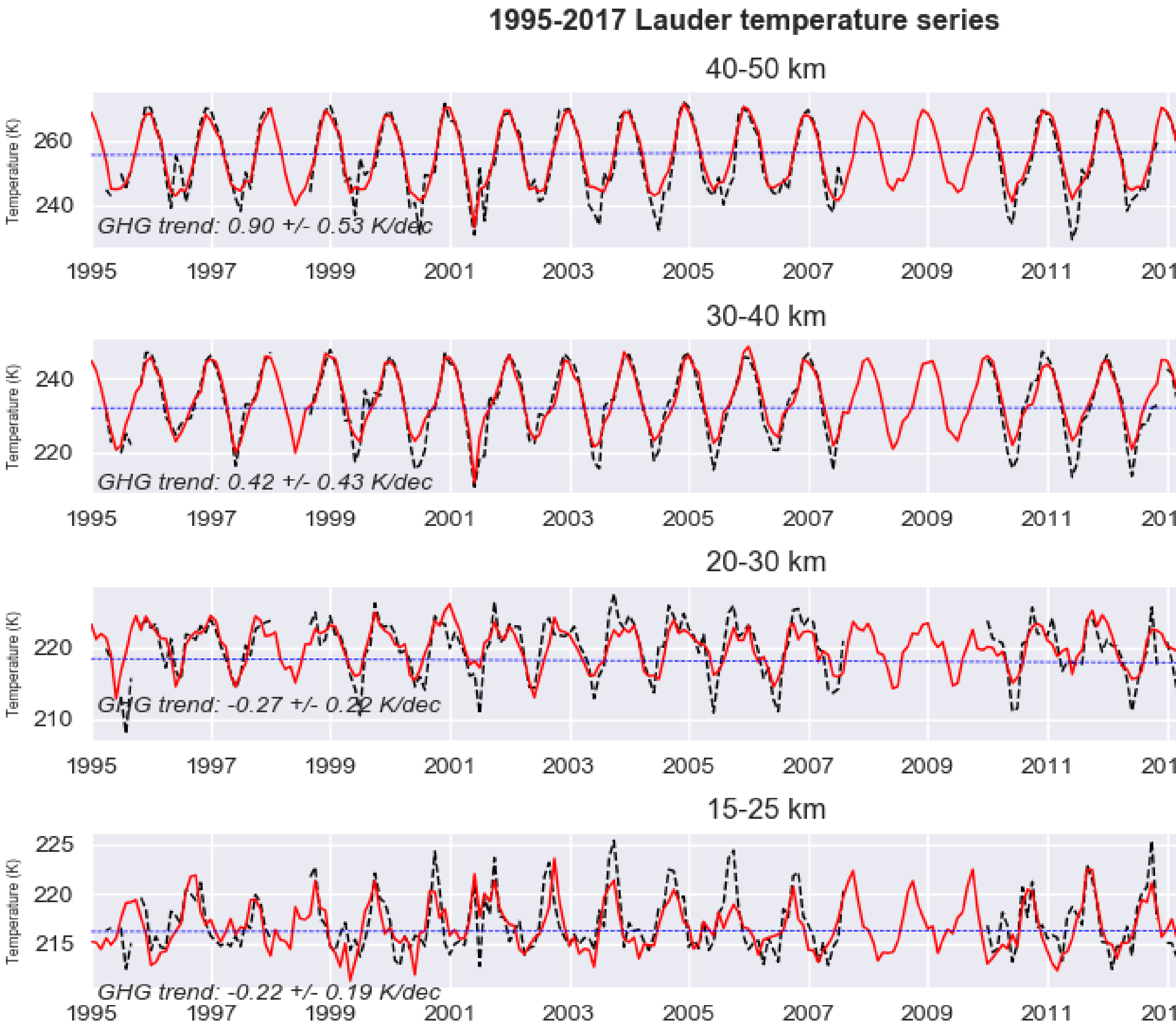

Figure 5.1: *Trend model results for the complete time series for Lauder after EOF dimension reduction.*

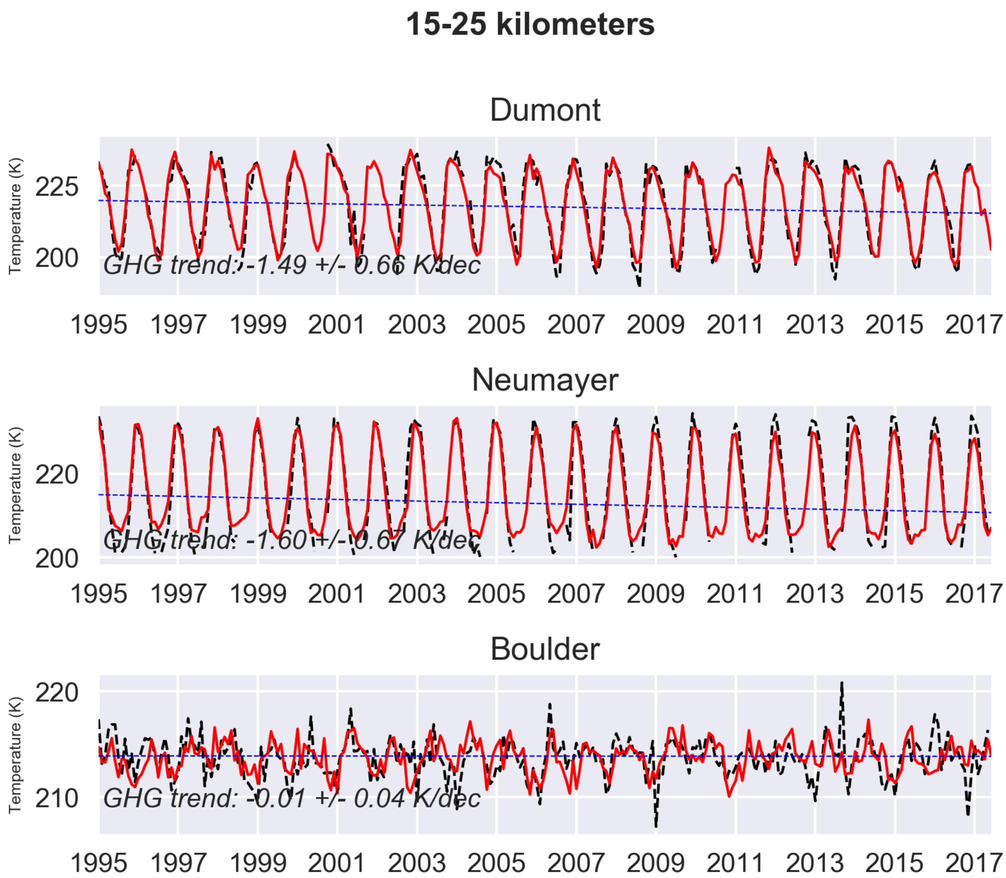

Figure 5.2: *Trend model results for the complete time series for Dumont, Neumayer and Boulder for the 15-25 km altitude bin. After EOF dimension reduction.*

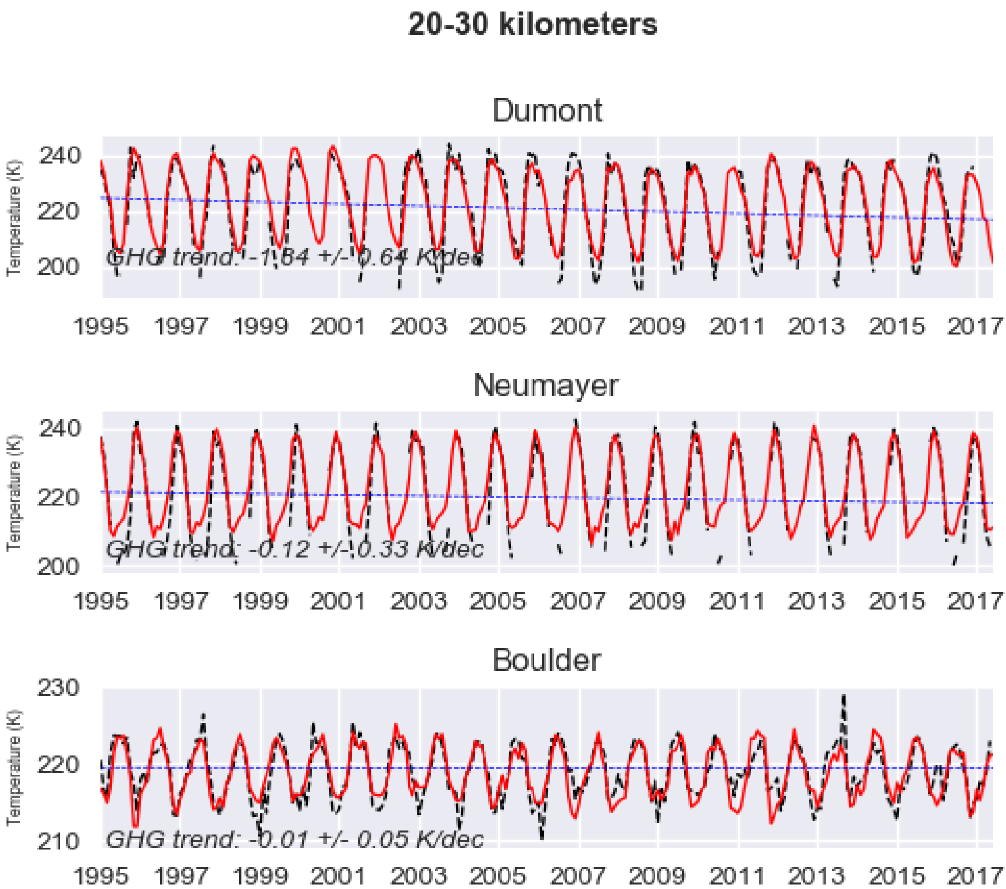

Figure 5.3: *Trend model results for the complete time series for Dumont, Neumayer and Boulder for the 20-30 km altitude bin. After EOF dimension reduction.*

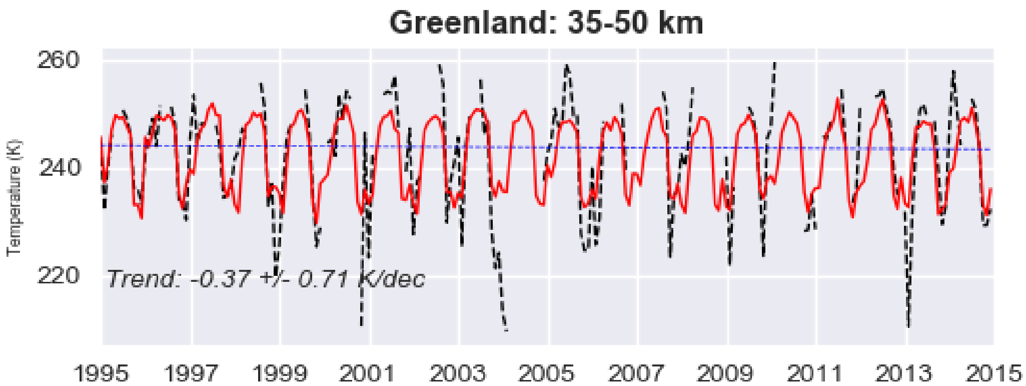

Figure 5.4: *Trend model results for the complete time series for Greenland for the 35-50 km altitude bin. After EOF dimension reduction.*